

# The role of bioelectrical patterns in regulative morphogenesis: an evolutionary simulation and validation in planarian regeneration

Sammy Hansali<sup>+</sup>, Léo Pio-Lopez<sup>+</sup>, Jennifer V. Lapalme<sup>†</sup> Michael Levin

**Abstract**—Endogenous bioelectrical patterns are an important regulator of anatomical pattern during embryogenesis, regeneration, and cancer. While there are three known classes of instructive bioelectric patterns: directly encoding, indirectly encoding, and binary trigger, it is not known how these design principles could be exploited by evolution and what their relative advantages might be. To better understand the evolutionary role of bioelectricity in anatomical homeostasis, we developed a neural cellular automaton (NCA). We used evolutionary algorithms to optimize these models to achieve reliable morphogenetic patterns driven by the different ways in which tissues can interpret their bioelectrical pattern for downstream anatomical outcomes. We found that: (1) All three types of bioelectrical codes allow the reaching of target morphologies; (2) Resetting of the bioelectrical pattern and the change in duration of the binary trigger alter morphogenesis; (3) Direct pattern organisms show an emergent robustness to changes in initial anatomical configurations; (4) Indirect pattern organisms show an emergent robustness to bioelectrical perturbation; (5) Direct and indirect pattern organisms show a emergent generalizability competency to new (rotated) bioelectrical patterns; (6) Direct pattern organisms show an emergent repatterning competency in post-developmental-phase. Because our simulation was fundamentally a homeostatic system seeking to achieve

This paragraph of the first footnote will contain the date on which you submitted your paper for review, which is populated by IEEE. This work was supported in part by the Templeton World Charity Foundation via grant TWCF0606. (*Corresponding author:* Michael Levin).

S. Hansali (e-mail: [sammy.hansali@tufts.edu](mailto:sammy.hansali@tufts.edu)) and L. Pio-Lopez (e-mail: [leo.lopez@tufts.edu](mailto:leo.lopez@tufts.edu)) are with the Allen Discovery Center at Tufts University, Medford, MA, 02155 USA.

J. V. LaPalme is with the Allen Discovery Center of Tufts University, Medford, MA, 02155 USA; and the University of Massachusetts School of Medicine, Worcester, MA 01655 (email: [jennifer.lapalme@umassmed.edu](mailto:jennifer.lapalme@umassmed.edu)).

M. Levin is Director of the Allen Discovery Center at Tufts University, Medford, MA, United States; and is associate faculty at the Wyss Institute of Biologically Inspired Engineering at Harvard University (email: [michael.levin@tufts.edu](mailto:michael.levin@tufts.edu)).

<sup>+</sup> These authors contributed equally to this work.

Mentions of supplemental materials and animal/human rights statements can be included here.

Color versions of one or more of the figures in this article are available online at <http://ieeexplore.ieee.org>

specific goals in anatomical state space (the space of possible morphologies), we sought to determine how the system would react when we abrogated the incentive loop driving anatomical homeostasis. To abrogate the stress/reward system that drives error minimization, we used anxiolytic neuromodulators. Simulating the effects of selective serotonin reuptake inhibitors diminished the ability of artificial embryos to reduce error between anatomical state and bioelectric prepattern, leading to higher variance of developmental outcomes, global morphological degradation, and induced in some organisms a bistability with respect to possible anatomical outcomes. These computational findings were validated by data collected from *in vivo* experiments in SSRI exposure in planarian flatworm regeneration.

**Index terms**—bioelectricity, bistability, evolution morphogenesis, neural cellular automata

## I. Introduction

Morphogenesis, a central aspect in developmental biology, is the processes that governs the formation and development of an organism's large-scale structural features. These processes involve large numbers of cells that create and repair a species-specific target morphology[1]. Understanding this process is critical for advancing the study of evolutionary developmental biology and for pioneering new approaches in regenerative medicine. Specifically, knowledge of how groups of cells interpret biophysical signals to determine the anatomical structure they will cooperate toward is crucial for addressing issues like birth defects, recovery from traumatic injuries, degenerative diseases, cancer, and aging.

One complex and poorly understood aspect is the cessation of growth once the desired structure is fully formed. For instance, axolotls can regenerate perfect replicas of lost limbs, tails, eyes, jaws, and other body parts, with growth and remodeling halting precisely when the correct form is achieved[2,3]. Moreover, regulative morphogenesis can reach the target morphology whether the starting point is a typical anatomical scenario or a novel configuration. For

instance, tadpoles that start with experimentally-induced disordered placements of craniofacial features still develop into normal frogs[4,5]. This occurs because the eyes, nostrils, and mouth shift along unconventional paths from their initial, misplaced positions to align correctly with standard frog anatomy. This ability is often described as a form of anatomical homeostasis, where deviations from the intended morphology are gradually corrected to achieve the desired anatomical structure, or in other words progressively reducing the error between the current state and a specific anatomical setpoint (the target morphology)[6,7].

In regeneration as well as embryonic development, complex species-specific structures must be formed *de novo*. The space of possible geometric layouts (anatomical morphospace) is enormous[8-11]; crucially, most species are able to achieve not only increase of complexity during morphogenesis, but in fact context-specific repair and novel collective behaviors in the face of unexpected perturbations[6,12]. How do cellular collectives reliably navigate morphospace [13] to form correct anatomical structures in both natural and unexpected scenarios? Cells coordinate their actions during morphogenesis through a mix of chemical, biomechanical, and bioelectrical signals[11,14-18] (see Figure 1). Rather than a precise anatomical blueprint, the genome provides the cellular building blocks, such as proteins, and sequence-specific regulatory information that can be modeled as gene regulatory networks. It's the role of developmental physiology to translate this information into morphogenetic actions of groups of cells that reliably achieve anatomical outcomes.

While a number of biophysical and biochemical modalities can be explored computationally, here we focus on one specific layer of that control information: bioelectrical prepatterns[19-22], e.g. ion gradients or spatiotemporal distributions of resting potential, established by ion channels and shaped by electrical synapses known as gap junctions (see Figure 1). Gap junctions can transmit molecules with a size cutoff of <1.2 kDa in size, and are gated by a number of cellular factors [23,24] which allow them to act as versatile valves that establish iso-potential compartments of cells that correspond to organ and tissue boundaries in morphogenesis[25-33]. Together, the action of ion channels and gap junctions gives rise to slowly changing physiological states that serve as prepatterns to domains of gene expression and ultimately anatomy.

Developmental bioelectricity refers to the endogenous electric potentials that are generated within cells and tissues, which are essential for coordinating cellular activities and control the large-

scale patterning of anatomical structures (reviewed in[14,23,24]). Non-neural bioelectric signaling has now been implicated in embryogenesis, regeneration, and cancer suppression (reviewed in[14,19,21]). Bioelectric properties determine the prepatterns of gene expression and tissue form in the formation of complex structures such as the vertebrate face[25-27], axial patterning of the dorso-ventral[28], anterior-posterior[29,30], and left-right [31,32] axes, the location and identity of specific organs such as the eye[33,34], the wing[35-38], and the egg-ovary system[39-43], patterning of skin and feathers[44], and size control[45-49]. Numerous transcriptional [50] and epigenetic [51] targets lie downstream of changes in bioelectric state. Several transduction mechanisms have been identified which convert changes in resting potential to alterations in gene expression, including calcium signaling and the regulation of movement of serotonin through gap junctions and through voltage-sensitive serotonin transporters[52,53]. Computational modeling has been applied to understand how bioelectrical changes propagate through tissues and over time, by simulating the feedback loops by which ion channel activity changes resting potentials which in turn can open and close gap junctions, leading to complex dynamics[54-56].

One of the major open areas of research concerns the ways in which large-scale (not single cell) bioelectric properties contribute to the ability of cell collectives to reliably achieve their correct target morphology, and a number of computational simulations have attempted to shed light on this process in planaria[57,58]. The Planarian flatworm is a popular model system for the study of both, regenerative anatomical homeostasis and bioelectric signaling[59,60]. Normal planaria have a very stereotypical anatomical layout, with a prominent anterior-posterior axis that has a tail at one end and a head (with brain and eyes) at the other end. When cut into pieces, each regenerates a precisely correct, allometrically scaled, little worm[61,62]. It has now been shown that planaria exhibit a notable prepattern of resting potentials with a depolarized region indicating where the head(s) should be built[29,63,64]. This gradient is instructive for the anterior-posterior axis and the number of heads, because modulation of that basic pattern (via targeting ion channels and gap junctions) can be used to produce 2-headed animals in the absence of any genetic or transcriptional manipulations[65]. Thus, the bioelectric control of head position and number[30,63], as well as size [66] and shape[67], in planaria are an example of how bioelectric patterns in tissue serve as a reference point

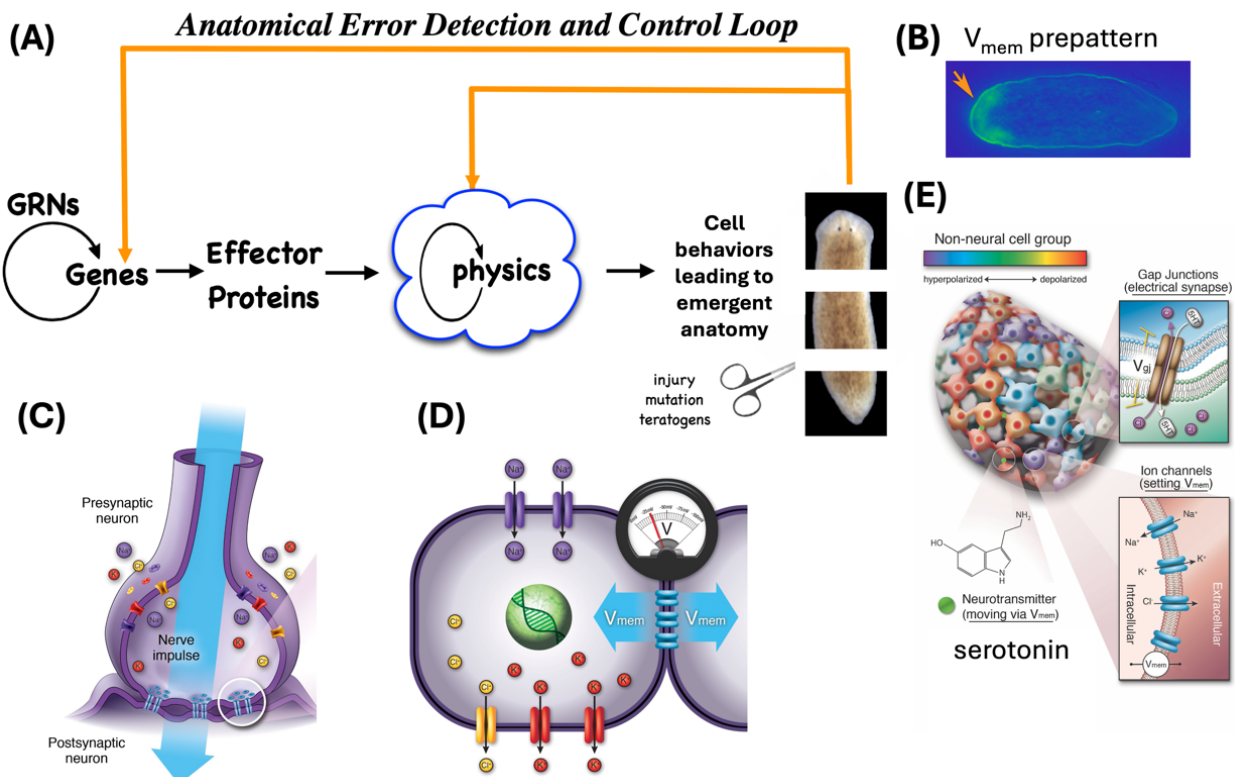


**Figure 1.** A) Scheme of anatomical homeostasis. Morphogenesis is not just a straightforward emergent process but represents the adaptive capability of living systems to modify and reorganize toward defined target structures. Achieving this requires feedback mechanisms at both the transcriptional and biophysical levels, which depend on stored information (such as bioelectrical pattern memories) to minimize errors. B) Voltage gradient across the anterior/posterior axis of planarian flatworms, visualized by a bioelectric reporter dye, which determines the location and number of heads (orange arrowhead indicates depolarized region which will develop a head). C) Neural cells form interconnected networks in which ion channels establish specific resting membrane potentials and enable selective communication with neighboring cells through gap junctions. This coordinated activity of ion channels and gap junctions underlies the neuronal signaling essential for cognition and behavior, allowing voltage potentials to be set and propagated throughout neural networks. D) Cells possess ion channels and are connected by gap junctions, forming a bioelectrical network outside the brain. Ion flow through these channels establishes the resting membrane potential ( $V_{mem}$ ), which is transmitted to neighboring cells via electric synapses. This system enables cellular communication and coordination, with neural dynamics serving as an advanced version of this fundamental mechanism. E) Ion channel proteins regulate ion movement and establish resting membrane potentials ( $V_{mem}$ ), which are communicated through gap junctions to create stable  $V_{mem}$  distributions within tissues, e.g. ion gradients. By targeting ion channels, gap junctions, and neurotransmitter signaling using methods like optogenetics, mutations, and pharmacological agents, researchers can modify bioelectric gradients. These alterations influence gene expression and cell behavior, guiding morphogenetic processes such as organogenesis. Images in panels A, C, D taken with permission from [70]. Images in panel B taken with permission from [63]. Image in panel E taken with permission from [1]. Images in C,D,E provided by Jeremy Guay of Peregrine Creative.

for morphogenesis (see Figure 1) – they encode information about the target morphology which the regenerative error minimization process uses as a setpoint to guide (and eventually cease, when the target has been met) its activities.

To increase impact of bioelectric modulation in fields like cancer, regeneration, embryonic malformations and aging[68,69], as well as in bioengineering, it is essential to crack the bioelectric code[70]. This means, moving beyond existing information on how voltage levels manipulate cell-level second messengers and regulate gene expression

[20,38,46-48,71-74] and stem cell behavior [75-78] to achieve a computational understanding of how specific bioelectric patterns map onto anatomical outcomes. Such knowledge could then be used to derive efficacious interventions for biomedical settings[79-81], as well as a better understanding of the contribution of bioelectric pattern control mechanisms in an evolutionary-developmental biology context[67].

The key to understanding any biological code lies in deciphering how it is read or decoded [82-85] — what information does it contain and how is this information

TMBMC-TPS-25-0025

interpreted by cells and tissues? The bioelectric code has been shown to operate through at least three main types of patterns: directly encoding, indirectly encoding, and discrete triggers[86]. Directly encoding pre-patterns map 1:1 with the specific target morphology that they encode. For example, the “Electric Face” is a pre-pattern that arises during embryogenesis of *Xenopus laevis* and instructively demarcates the location of future tadpole facial structures[26]. It is a direct pattern because the regions of bioelectric state indicate, in a clear way, the actual locations of the craniofacial organs.

In contrast, indirectly encoding pre-patterns do not map to the specific structures that they encode in any obvious manner. For example, a specific  $V_{mem}$  pattern induces the growth and patterning of a new tail [87]. Similarly, a  $V_{mem}$  gradient controls the size [66] and specific shape [27] of planarian head regeneration. In both of these cases, bioelectric pre-patterns specified growth of structures whose geometry could not have been guessed by inspection of the bioelectric pre-pattern – the voltage patterns don’t look like the anatomy they encode.

Finally, trigger pre-patterns have even less similarity to the final outcome: they do not seem to encode specific structures and are very low information-content stimuli. Instead, they can initiate comprehensive morphogenetic programs that result in the formation of complex structures (such as organs and appendages) without requiring micromanagement of the specific structure. For example, inducing sodium influx or proton pumping to tadpole limb or tail amputation sites has been shown to trigger the regeneration of the entire appendage—with correct vasculature, innervation, and muscle—even during periods when such regeneration is not typically possible[88]. And, the same stimulus (triggered by the ionophore monensin) induces tails in a tadpole and legs in a froglet – the specificity is not in the signal but in the interpretation machinery triggered by it[89]. These examples indicate that bioelectric patterns can serve as master regulators, kick-starting the growth of complex structures, and all the myriad required molecular processes, from a relatively simple upstream event that itself doesn’t have the informational bandwidth to specify the details.

While computational models exist of bioelectrical dynamics[54,56,90,91], there are currently no computational platforms that facilitate the study of the different modes of bioelectrical encoding in the context of morphogenesis, to generate testable predictions about interventions and these decodings’ evolutionary properties. To bridge these knowledge gaps, we built simulation software that enables exploration of how artificial organisms develop morphogenetic competencies over developmental and

evolutionary timescales with the different types of bioelectrical patterns.

We employed evolutionary algorithms to simulate the evolution of a neural cellular automata (NCA) [92-95] model for regulative morphogenesis, and studied its various properties under the 3 different models of bioelectric encoding. We found that: (1) All three types of bioelectrical codes allow the reaching of target morphologies; (2) The resetting of the bioelectrical pattern and the change in duration of the binary trigger alter morphogenesis; (3) The direct pattern organisms show an emergent robustness to changes in initial anatomical configurations which we did not explicitly reward for during evolution; (4) The indirect pattern organisms show an emergent robustness to bioelectrical perturbation; (5) Direct and indirect patterns organisms show an emergent generalizability competency to new bioelectrical patterns obtained via rotation of the original ones; (6) Direct patterns organisms show an emergent repatterning competency in post-developmental phase. Because our simulation was fundamentally a homeostatic system seeking to achieve specific goals in anatomical state space, we sought to test the effects of anxiolytics that reduced concern over the distance to those goals. Specifically, given the hypothesis that stress/reward is a driver of progressive error reduction during morphogenesis[96,97], we focused on neuromodulators that inhibit the homeostatic loop by abrogating the stress/reward system. We developed a selective serotonin reuptake inhibitor simulation, which predicted a diminished ability of artificial embryos to reliably achieve morphogenetic outcomes, leading to higher variance of developmental outcomes, global morphological degradation, and anatomical bistability. These computational findings were then validated by wetlab data collected from planaria regenerating with SSRI exposure.

## II. RELATED WORK ON ARTIFICIAL EMBRYOGENY

The field of artificial embryogeny has been historically centered on the French flag model [98-101], with a focus on how cells interpret positional information and differentiate into specific cell types based on morphogen concentrations to form a specific anatomy. This model relies on the existence of thresholds in the morphogen gradient to guide cell fate determination and spatial patterning. The foundational work of Lewis Wolpert introduced the French Flag model, which explained how morphogen gradients can provide positional information to cells, resulting in distinct cellular fates based on concentration thresholds[99]. Subsequent studies have developed mathematical and computational models to simulate

the French Flag pattern formation. For example, Bowers [102] demonstrated the formation of modular structures in a computational evolutionary model of embryogeny, highlighting the phenotypic robustness in generating French flag-like patterns[102]. Recent studies have integrated the French Flag model with other theoretical frameworks in developmental biology, such as the Turing mechanism of pattern formation and gene regulatory networks. These integrative approaches have provided deeper insights into the robustness and flexibility of developmental patterning mechanisms[103]. Other work also included growth and repair simulation models, reaction-diffusion experimental models, and computational frameworks that aim to create robust and tunable axial patterns[103-105]. Chavoya and Duthen utilized a genetic algorithm to evolve cellular automata capable of generating various two-dimensional and three-dimensional shapes. They also evolved an artificial regulatory network (ARN) to generate cell patterns, effectively addressing the French flag problem[106,107]. The French flag problem has also been studied in the context of self-organizing paradigms, where the challenge lies in achieving robust and tunable axial patterns without the need for global signaling cues[108]. The French Flag model remains a pivotal framework in developmental biology and artificial embryogeny, facilitating our understanding of how cells interpret positional information to create intricate patterns during development.

Recently, Neural Cellular Automata (NCA) models have been introduced in the field of in silico embryogeny[97,109-112]. Pio-Lopez et al. conducted a study on the scaling of goals from cellular to anatomical homeostasis using evolutionary simulations to resolve the French-flag problem[97]. The results suggested that the collective problem-solving of cells during morphogenesis can evolve into traditional behavioral intelligence by scaling up during evolution homeostatic competencies via stress sharing in metabolic space. Grasso (2022) explored the concept of Empowered Neural Cellular Automata in the context of morphogenesis. The study found that incorporating empowerment as a secondary objective in the evolution of NCA for morphogenesis tasks leads to higher fitness compared to evolving for morphogenesis alone[109]. This highlights the importance of incorporating empowerment as a guiding principle to enhance the efficiency and effectiveness of NCA in performing morphogenetic tasks. Very recently, Hartl et al. developed an NCA implementing a multi-scale competency architecture to resolve a more complex version of the French flag model, the Czech flag and a smiley face as another target morphology[110]. Other works extended

modelling approach of morphogenesis with NCAs to the encoding of a manifold of NCA, each of them capable of generating a distinct image[113], growing 3D shapes[114], or hierarchical NCAs for morphogenesis[115].

However, none of these models incorporated the use of the bioelectrical pattern for regulating morphological behavior. Manicka et al. studied how non-neural cells collectively make decisions in the context of morphogenesis, by constructing a minimal biophysical model of a bioelectric network that integrates fundamental components and processes of bioelectrical signaling[116]. Although computational models of bioelectrical dynamics exist[54,56,90,91], there is no platform to analyze modes of bioelectrical decoding by cell groups in morphogenesis, or to predict their evolutionary effects. To fill this gap, we created simulation software by extending previous work using evolutionary NCA for morphogenesis[97,110], that explores how artificial organisms develop morphogenetic abilities over developmental and evolutionary times, driven by different types of bioelectrical patterns: direct, indirect and the binary trigger.

### III. MATERIALS AND METHODS

#### A. *In-silico evolutionary system for bioelectrically-regulating morphological Behavior*

We simulated the evolution and development (Figure 2) of 9x9 cells artificial organisms on a morphogenetic task driven by different types of bioelectrical patterns using a genetic algorithm. Using this simulation, we aimed to gain insight on how biological organisms utilize bioelectric patterns during pattern formation and morphogenesis during regulative development, as well as to explore the developmental properties that emerge from organisms evolved with three classes of bioelectric patterns. Due to the large space of possible anatomies that exist in nature, we simplified the model to explore the development of two organisms (the “Tadpole”, inspired by Vandenberg et al.’s tadpole craniofacial rearrangement experiment[117], and the “French Flag”, as described by Wolpert’s original French flag problem[98,99]), each with their own starting and target morphologies. The bioelectric patterns were designed by us, so that we could test our hypotheses on the emergent properties of organisms utilizing various patterns. As with all computational models of biology, we made choices about which features to simulate, and did not explicitly include all the

TMBMC-TPS-25-0025

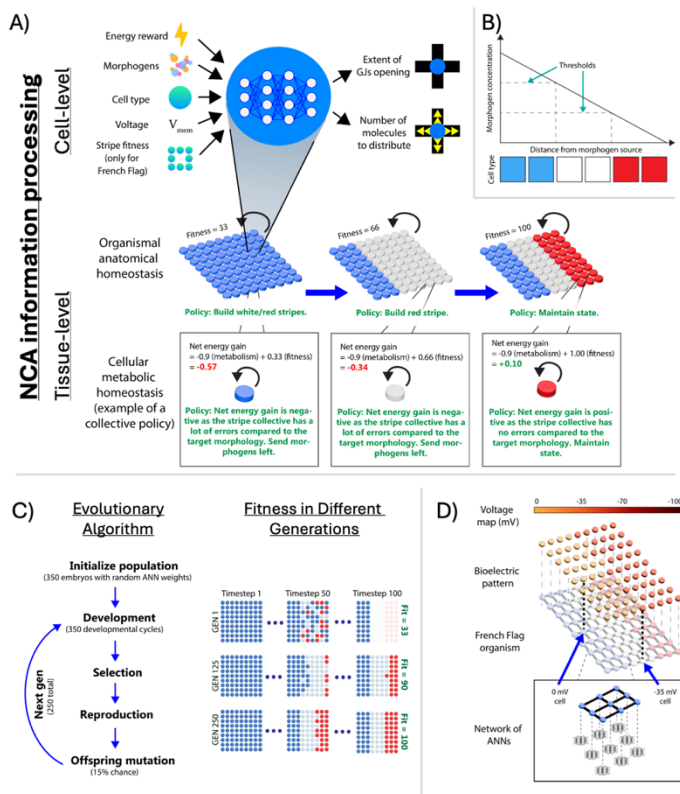


**Figure 2. Representation of the NCA system.** A) NCA information processing occurs at the tissue and cellular levels. At the cell level, cell ANNs take inputs of energy, molecule amounts, cell type, voltage, and (for French Flag axially patterned organisms only) the average cell types of neighbors. They output the cell's actions – how much to open gap junctions and what number of molecules to distribute. At the tissue level, anatomical and metabolic homeostasis are integrated. Organisms perform anatomical homeostasis to maximize fitness by following policies such as “Build a red stripe”. Cells perform metabolic homeostasis to maintain positive energy levels by following policies such as “Send molecules left”, following the policy of the organism. B) Description of the original French Flag Problem. The concentration of the morphogen as it diffuses left to right across the tissue conveys positional information, which is interpreted by cells to determine their cell types. C) On the left is an overview of one evolutionary cycle. First, a population of 350 embryos is initialized with randomized weights. Next, the embryos are allowed to develop and are selected based on their fitness and allowed to reproduce. All offspring from the reproduction phase have a 15% random mutation chance, after which the next epoch begins, for a total of 250 epochs before evolution concludes. On the right is an example of what the highest fitness French Flag organisms would look like at each epoch. During the first generation, the highest fitness organism achieves a fitness of 33% by maintaining the blue stripe in the correct location. By generation 125, the best organism achieves a fitness of 90% by learning that there should be a central white stripe and rightwards red stripe. It hasn't learned that red stripes need a width of three. Finally, by the last generation, the best organism has learned to solve the French Flag morphology. D) Cellular bioelectricity and ANN. Each cell maps to a specific voltage ranging from 0 to -100mV (specified by the bioelectric pattern) and a cellular ANN.

mechanisms by means of which cells communicate, perceive and act on their environment, differentiate, and perform basic metabolic functions. While these details are important to biological systems, we did not require more advanced modeling to answer our specific questions.

The following sections detail the structure and behavior of our artificial organisms and cells, the developmental cycles that enable embryos to reach adult morphologies, the evolutionary cycles by which a population's best morphogenetic strategies are discovered, and the implementation of bioelectricity as

a goal-encoding layer that serves as the setpoint for the anatomical homeostasis process.

### 1. Organisms

Each digital organism possesses a distinct artificial neural network (ANN), similarly to the gene regulatory networks controlling the decision-making pathways in real cells[118]. Transcriptional networks and pathways are known to underlie a neural network-like architecture[119-126]. Organisms are

represented as 2-dimensional arrays of cells, depicted as colored circles, with each cell containing a copy of the ANN (see Figure 2D). Organisms have two stages: embryo and adult. The adult phase starts once the target morphology has been reached. Embryos are initialized as a 9 by 9 matrix of cells and undergo a developmental cycle to become an adult. Adults undergo fitness evaluations for selection at 100 steps.

There are two species of artificial organisms in this work: “Tadpole” and “French Flag” (Figure 3A). Tadpoles’ embryonic craniofacial morphology begins as deformed facial features but its adult morphology is a rearranged, symmetrical face, modeling the remarkable observed craniofacial repair of “Picasso tadpoles” [117] and the “electric face” prepattern known to drive face development[26]. This is a direct pattern and we used it to model this known biological phenomena, it is also more complex than the French flag morphogenetic problem. The embryonic morphology of French Flag organisms begins as an undifferentiated monolayer of blue cells, which develops into the likeness of the French Flag. This models Wolpert’s famous French Flag problem[99], in which 3 colors are used to represent three distinct cell types in a positional information axis. We used the pattern for the other type of patterns.

## 2. Cells

### Representation and attributes

Cells are represented as objects containing energy (a floating point number ranging between 0 and infinity, initialized at 50), molecules (a floating point number greater than or equal to 0, initialized to an amount depending on the starting cell type (Figure 3A), gap junctions (percentage between 0 (fully closed) to 100 (fully open), initialized at 0), a cell type that depends on the species (Figure 3A), a voltage (integer between 0 and -100, initialization depends), and an ANN [127] (Figure 2A).

An energy threshold greater than zero is required for cells to stay alive. At 0, the cells die. Molecules are exchangeable with neighboring cells and determine cell type. Gap junctions are channels between cells that regulate the flow of molecules according to their opening percentage. A cell’s type is its identity. The available cell types vary by species. Tadpoles possess 4 cell types (tan, red, black, and blue) while French Flags contain only three cell types (white, red, and blue) (Figure 3A). Voltage is another type of information that can be seen as a goal-encoding layer in the form of different bioelectrical patterns (direct, indirect and the binary trigger, see Figure 3B).

A)	Species	Embryonic Morphology	Target Adult Morphology	Cell Type	Molecules	Appearance
Tadpole				Tan	$0 \leq x < 5$	
				Red	$5 \leq x < 10$	
				Black	$10 \leq x < 15$	
				Blue	$15 \leq x$	
French Flag				White	$5 \leq x < 10$	
				Red	$10 \leq x < 15$	
				Blue	$15 \leq x$	

B)	Type of Bioelectric Pattern	Associated Species	Bioelectric Patterns Used
Direct	Tadpole		
Indirect	French Flag	Half & Half	
		Cross	
		Triangles	
		LL	
Binary Trigger	French Flag	Stage 1: Rest	
		Stage 2: Trigger	
		Stage 3: Rest	

**Figure 3. Embryonic morphologies, target morphologies and bioelectrical patterns.** A) Embryonic morphologies, target morphologies, cell types, and molecule thresholds for cellular differentiation for each species. B) Specific bioelectric (direct, indirect, binary trigger) patterns used for each type and species. There is only one type of direct pattern, four types of indirect patterns, and one type of binary trigger pattern (divided across 3 stages: rest, trigger, and rest). Whenever a direct pattern is used, it is for a Tadpole organism. Any other pattern (indirect or binary trigger) corresponds to a French Flag organism.

### Cellular perception-action cycle

An activated cell behaves in a precise series of steps, similar to Algorithm 1 from Pio-Lopez et al.[97]. First, a bias of 0.5 and cellular attributes from times  $t$  and  $t_{-1}$  are passed as inputs to the cell’s ANN, which then returns the outputs.

The inputs are energy and molecule levels, cell type, and voltage. In addition, French Flag cells have one extra input which is the current fitness of their stripe, similarly to[97].The outputs are the amount to open gap junctions and the number of molecules to distribute to neighboring cells (Figure 2A). These outputs are then processed by the cell’s communication module, similarly to Algorithm 2 from Pio-Lopez et al.[97]. The cell’s gap junctions are opened, and its molecules are transferred to the neighbors. The number of molecules distributed depends on both outputs. Molecules are distributed to neighboring cells in a randomized order. If the number of molecules a cell must distribute times the gap junction opening times the number of neighboring

TMBMC-TPS-25-0025

cells is greater than the cell's molecule stock, then the cell will keep distributing molecules until it runs out of molecules. Then, the cell differentiates into a new cell type if it has met the new cell type's threshold for molecules (Figure 3A). For details of various differentiation mechanisms explored in this work, look at (Supplementary Material, Figure S1). Every differentiation costs the cell 0.50 energy.

Cells have a metabolic cost for survival, between 0.65 and 0.95 energy per activation, depending on the difficulty of the learning task. This energy loss per activation is counteracted by an energy gain of between 0 and 1 energy per activation. This energy gain is in proportion to the organism's fitness at the beginning of the current timestep. Energy acts as a reward incentive for cells to cooperate towards correct morphogenesis. In sum, cells rapidly lose energy and die unless the organism reaches close to the target morphology by adulthood. Thus, an organism-level anatomical homeostatic loop is implemented from the binding of cellular-level metabolic homeostatic loops (Figure 3B).

### 3. Development and fitness

Each embryo underwent a 100 timestep developmental cycle into an adult. Organisms learned to differentiate their cells in a way that increases fitness. For every timestep in a developmental cycle, all cells are activated in a random order. At the end of the 100<sup>th</sup> timestep, the adult's fitness is evaluated out of 100 points. Fitness is quantified by how close the adult's morphology is to its pre-defined target morphology (either the Tadpole or the French Flag). Each species has its own specific fitness evaluation. For tadpoles, they received 30 points if the eyes are in the correct quantity and position, 28 points for the mouth, 6 points for the nose, and 36 points for the skin. Skin was weighted less to enable other organs to form despite the prevalence of skin cells.

For the French Flag, organisms receive a fitness score according to how much they reached the appropriate morphology with 33.3 points for each stripe being in the correct quantity and position, each stripe matters equally.

Overall, the use of the bioelectrical pattern is not rewarded in the fitness function. Organisms may or may not use it during evolution.

### 4. Evolution and genetic algorithm

Each population of organisms underwent a 250-generation evolutionary cycle, with each generation composed of hundreds of developmental cycles

(Figure 2C). A population contains 350 organisms. To create and evolve populations, we used the ES-HyperNEAT genetic algorithm (Evolvable-Substrate Hypercube-based NeuroEvolution of Augmenting Topologies)[128-130]. HyperNEAT uses geometric regularities of the task domain to evolve large-scale neural networks that emulate neural connectivity patterns in the brain[131], but cells in non-neural tissue have similar connectivity. ES-HyperNEAT is a neuroevolution algorithm designed to evolve large-scale artificial neural networks with complex, regular connectivity patterns. It builds upon the HyperNEAT framework, which uses Compositional Pattern Producing Networks (CPPNs) to indirectly encode the connectivity of neural networks based on the geometric coordinates of neurons in a predefined substrate. While HyperNEAT requires this substrate to be specified in advance, ES-HyperNEAT extends the approach by evolving the substrate itself. This is achieved by defining a continuous geometric space and using the CPPN's outputs to determine which regions of the space are sufficiently distinct to warrant the inclusion of new neurons. The method selectively grows the network by exploiting these functional variations, enabling the emergence of scalable and structured neural architectures without manual specification of network topology. By leveraging both indirect encoding and adaptive substrate generation, ES-HyperNEAT facilitates the evolution of high-dimensional networks with biologically inspired properties such as symmetry, modularity, and repetition.

There are several stages of evolution. First, a population of 350 organisms was initialized, each with different ANN weights. For each generation over 250 generations, each organism receives a fitness equal to the average fitness from three development cycles. Averaging fitness controls for intra-organism fitness variability stemming from random activation. The top 20% most fit organisms reproduce to populate the next generation. These offspring are also vulnerable to random mutations. We set an overall mutation rate of 15%. We allowed recurrent connections and a maximum depth for the ANN of 3 hidden layers.

### 5. Bioelectric patterns

Every cell of an organism is assigned a voltage integer. A bioelectric pattern is defined as the 2d-array of cell voltages that maps to an organism's 2d-array of cells (Figure 2D). Organisms may decide to use the bioelectric pattern present to them, or not, to achieve their morphogenetic goals during evolution. We did not force in the code or incentivize them to use their bioelectric patterns, in order to observe the

TMBMC-TPS-25-0025

evolutionary-developmental conditions necessary for the adoption of bioelectricity. Evolution decides on its own to use it or not.

There are three types of bioelectric patterns in this work: direct, indirect, and the binary trigger. They are named based on their relationship with the target morphology. Direct bioelectric patterns have voltages that map one to one with cell types. This is not the case for indirect bioelectric patterns. Binary triggers have a 5 timestep rest period, followed by a 20 timestep “trigger” period, followed by a rest period for the remainder of the simulation. The binary trigger has a homogenous voltage.

Tadpole organisms only had access to a direct pattern during evolution. And there are two sets of French Flag organisms: (1) those who had access to four indirect patterns, or (2) those who had access to one binary trigger pattern during evolution. All bioelectric patterns used for the evolutions are in Figure 3B.

We focused on bioelectricity in this study as we seek to understand the impact of the different bioelectrical patterns on regulative morphogenesis during development, but numerous other developmental mechanisms – including biomechanics, chemical gradients, etc. – could be included to determine whether and how these influence the evolutionary process.

### 6. Parameters and code access

Genetic algorithm parameters used in this work are the same as in the previous work[97]. All code used in this work is freely available at <https://github.com/sammyhansali/ScaleFreeCognition>. Agent-based modeling framework, Mesa [132,133], was used to visualize organismal development along with dashboards for tracking fitness, gap junction connectivity, molecule exchange activity, energy, and more. The MultiNEAT package was used to implement ES-HyperNEAT[127].

### B. Material and method for the planaria SSRI experiment

A clonal strain of *Dugesia japonica* was kept in Poland Spring Water (Framingham, MA, USA), and maintained as in [134] and was starved for >7 days before cutting, a standard method used in this model system to reduce variability of data by controlling for the metabolic status of individuals[134]. To assess the impact of transient fluoxetine treatment on bioelectric states, middle third (trunk) fragments from *D. japonica* were allowed to regenerate in a 2uM

Fluoxetine or Sertraline solution for 3 days, at which point the solution was washed out and the samples were placed in Poland Spring water for 1 week (at 13°C to prevent fissioning). They were then photographed and scored for the number of heads, and to identify any changes in head morphology (which were not observed). Scoring was performed under a Zeiss SV6 dissecting microscope.

### III. SIMULATION RESULTS FOR THE 3 TYPES OF BIOELECTRICAL PATTERNS TO REACH A TARGET MORPHOLOGY: DIRECT, INDIRECT AND BINARY TRIGGER

#### A. All three types of bioelectrical codes allow the reaching of target morphologies.

To determine whether the artificial organisms learned to navigate the morphospace by following the bioelectric information available to them, we trained population of organisms per conditions (20 organisms for the direct bioelectrical pattern, 20 organisms by patterns for the indirect patterns organisms and 20 for the binary trigger organisms). Each species determines the embryonic morphology, target morphology, and cell types (Figure 3A) for the developmental task of that trial (tadpole for the bioelectrical pattern, French flag for the indirect and binary triggers). Each trial was repeated at least 20 times.

We found that at population level of the direct pattern organisms, the fitness is on average of 91 ( $\sigma=5\%$ ) demonstrating a good solution of the morphological task using direct pattern encoding in tadpole organisms (Table 1). In the representative direct pattern example shown in Figure 4A, the organism was able to reach the target morphology and achieved a fitness of 91.4 ( $\sigma=11.2\%$ ) over 20 developmental runs of the same organism. It displayed an initial burst of molecule exchange activity that set the stage for organogenesis. This was preceded by all of its gap junctions opening fully for one timestep, before closing off by 80% for the rest of the simulation. By time 50, the location for the future eyes, nose, and mouth were demarcated. By time 75 and 100, the resolution of the face increases. Activity plateaued over time as fitness increases and error decreases. Notably, the organisms reached a perfect fitness of 100, by time 200, demonstrating allostasis and stability capabilities seen in the previous similar models[97]. This is a common strategy for direct pattern organisms, especially with the gap junction opening fully for 1 timestep before closing off dramatically for the rest of the developmental period. Some direct organisms deviated from this strategy and

Species	Type	Bioelectric Pattern	Fitness		Resetting		Robustness to Initial State Configurations		Cut Robustness		Noise Robustness		Generalizability		Repatterning	
			Avg	Std	Avg	Std	Avg	Std	Avg	Std	Avg	Std	Avg	Std	Avg (200)	Std (200)
Tadpole	Direct	Direct	91	5	0	0	65	16	-	-	-	-	83	9	22	33
French Flag	Indirect	Half and Half	83	3	31	24	20	12	31	31	47	26	57	20	13	14
		Cross	77	3	51	16	6	11	42	29	43	24	27	7	7	11
		Triangles	80	5	48	15	2	4	43	32	41	27	24	2	1	3
		"LL"	78	4	52	17	1	2	40	32	44	27	23	3	0	0
		Avg of Indirect Patterns	79.5	3.75	45.5	18	7.25	7.25	39	31	43.75	26	32.75	8	5.25	7
	Binary Trigger	Binary Trigger	81	5	58	27	-	-	-	-	-	-	-	-	-	-

**Table 1. Population statistics for species of direct, indirect and binary trigger organisms.** From left to right, data is shown for organism fitness in standard conditions and the six key experiments: resetting of the bioelectric pattern, morphological robustness, bioelectric (cut and noise) robustness, generalizability, and repatterning. Population fitness scores are on a scale of 0-100%, where 0 means no one survived and 100 means all organisms achieved the target morphology.

instead learn to assign gap junction opening amounts specific to each cell type.

At the population level for the indirect bioelectrical pattern organisms, the fitness scores were: 83 ( $\sigma=3\%$ ) for "Half and Half" bioelectrical pattern, 77 ( $\sigma=3\%$ ) for "Cross", 80 ( $\sigma=5\%$ ), for "Triangles", and 78 ( $\sigma=4\%$ ) for "LL" (Table 1 and Figure 3B for the indirect bioelectrical patterns). Overall, the morphological task is harder than with the direct bioelectrical pattern with an average fitness among all indirect patterns of 79.5 (Table 1). The representative indirect pattern example (Figure 4B), which utilized a "Triangles" pattern, was also able to complete the developmental task. It achieved a maximum fitness of 96% during development and a fitness of 80.9 ( $\sigma=5.2\%$ ) over 20 runs. From timestep one onwards, its gap junctions were permanently open and molecule exchange was frequent. By the time 25 the blue stripe is clearly demarcated. By 75, the French flag starts to become discernable as the red cells colonize the right stripe. Finally at step 100, following several spikes of activity, the target morphology is realized with an error of 7 cells in the red stripe.

Finally, at population level of the binary trigger organisms (Figure 5C), the fitness is on average of 81 ( $\sigma=5\%$ ) (Table 1). In the example displayed in Figure 4C, we found that it solved the French flag with a fitness of 80.4 ( $\sigma=4.2\%$ ) over 20 runs. It immediately focused on isolating the blue stripe and white stripe, usually achieving that by the end of the binary trigger, step 25. From then on, its strategy was more stochastic. The organism started to have a three-cell wide red stripe on the right side, but it was not successful at retaining the red stripe for a long period. But it was enough to reach 90 fitness in the developmental run shown in Figure 4C. The cells repeatedly differentiated from white to red and red to blue. This strategy essentially continued in the post-

developmentary period, causing the decay of the tissue by step 200. Generally, there are two types of binary trigger organisms we observed. Those that began development before the binary trigger was presented at time 5, and those that began at time 5.

Thus, organisms with all three types of bioelectric patterns learned to navigate anatomical space to develop from early-stage embryo to the adult target morphology using their bioelectrical pattern. However, the task is much harder for the indirect patterns organisms and the binary trigger compared to the direct pattern organisms given their fitness difference, probably as learning a direct mapping is a linear task easier than learning an indirect one, with a non-linear relationship.

#### B. Regulative morphogenesis depends fully on the direct pattern, partially for the indirect pattern, and depends on the duration of the pattern for the binary trigger.

The digital organisms can reach their anatomical goals via high-level bioelectric patterning information. However, we did not specifically reward for utilization of bioelectricity data because we wanted to understand the developmental conditions which may have caused cellular collectives, over the course of evolution, to co-opt spatial gradients of membrane voltages for the purpose of morphogenesis. Without forcing the adoption of bioelectricity, would artificial organisms learn on their own to utilize bioelectric patterns to traverse anatomical space, or rely on the other ANN inputs (energy, molecules, cell type)?

In order to answer this question, we devised the "Resetting Bioelectricity" experiment (Supplementary Material, Figure S2). We reset the native bioelectric pattern of artificial embryos to a

TMBMC-TPS-25-0025

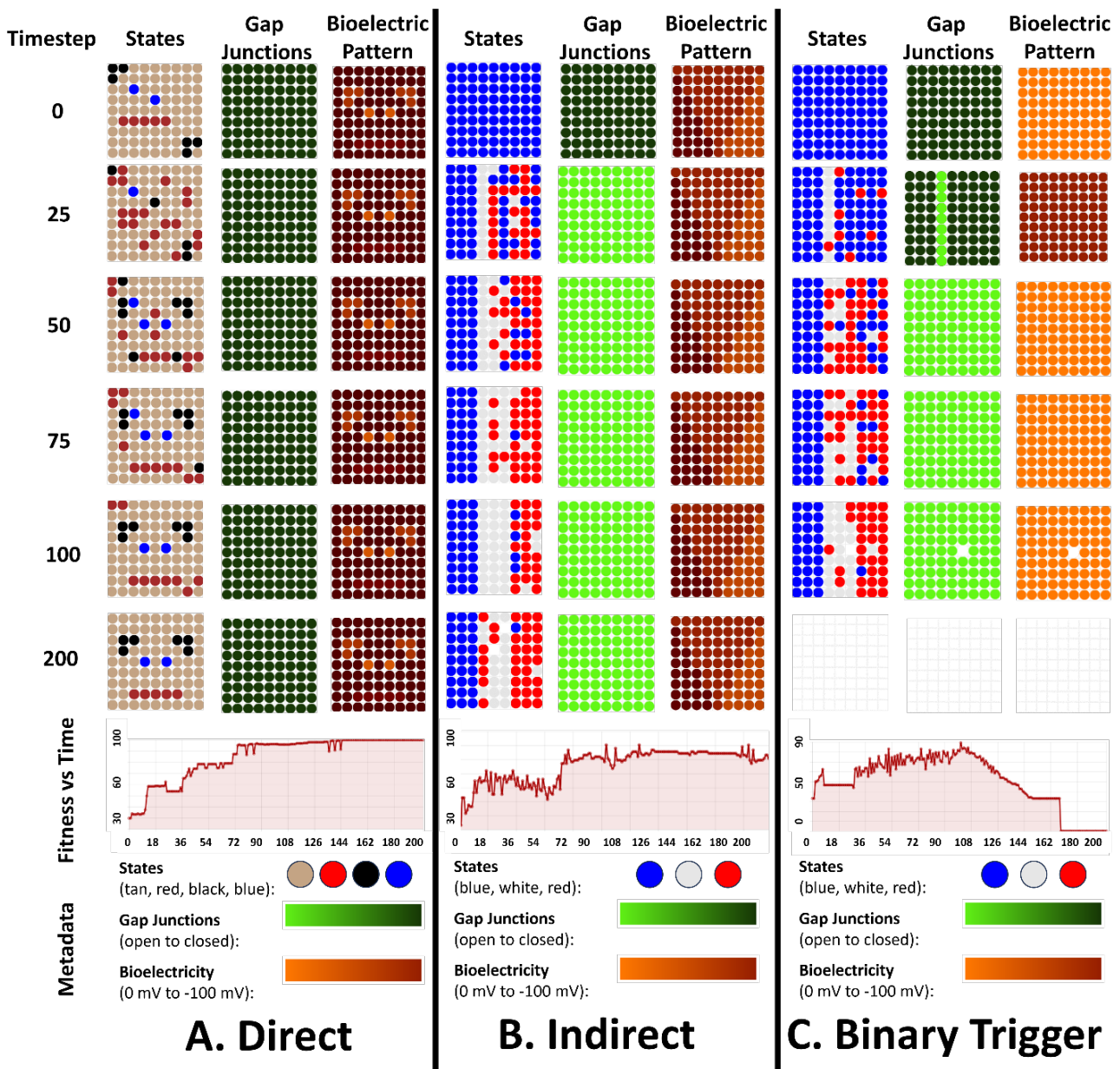


**Figure 4. All types of bioelectrical patterns allow the reaching of target morphologies.** Shown for each category are the temporal dynamics of cell states, bioelectrical input, and gap junctions used across 200 timesteps, sampled at six timesteps ( $T=0, 25, 50, 75, 100$ , and  $200$ ). Under that are the corresponding fitness vs. timestep chart. Finally, under that is the scales for states, molecules, gap junctions, and bioelectricity. A, B, and C are examples that show a single successful example for each Direct, Indirect, and Binary Trigger organismal development in standard conditions. A) Direct pattern organism example) Activity plateaus over time as fitness increases and error decreases. Notably, the organism's fitness steadily increases after the normal developmental period. B) Indirect pattern organism example. Activity is high in the early stages of development when fitness is low, and error is high. By step 108, past the normal developmental period, activity halts and fitness stagnates. By step 200 the tissue has started degrading and fitness steadily decreasing. C) Binary trigger organism example. Activity is characteristically high from timesteps 5 to 25, when the binary trigger pattern is present. Gap junctions immediately open in the first-time step. Like some other artificial organisms, fitness steadily decreases after the normal development period.

TMBMC-TPS-25-0025

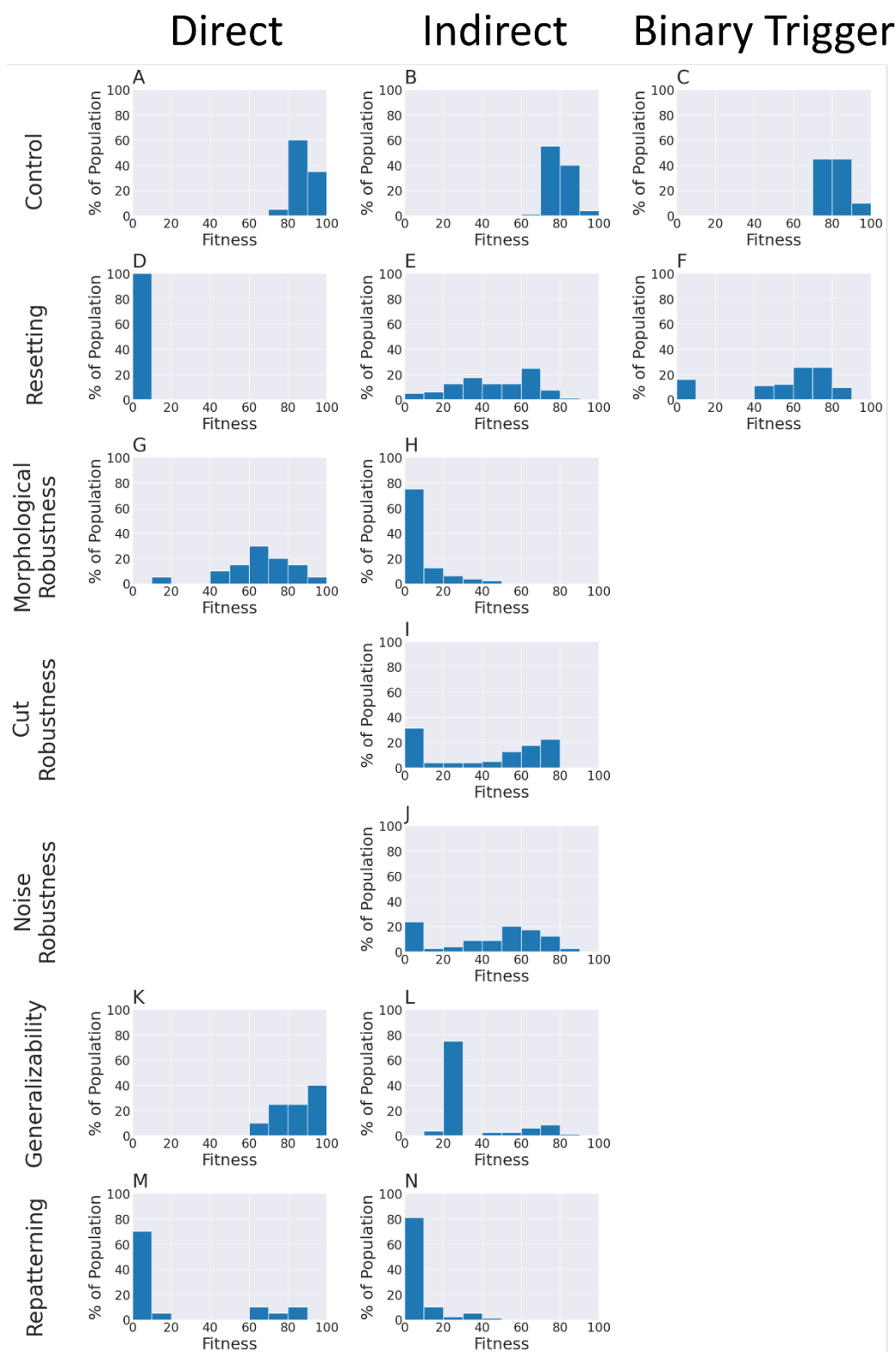


**Figure 5. Population-level fitness score distributions for the various experiments from Table 1.** Direct histograms have a population size of  $n=20$ , indirect histograms aggregate the fitness scores from all four indirect patterns (each has  $n=20$ ) for a total of  $n=80$ , and binary trigger organisms have a total of  $n=20$ .

TMBMC-TPS-25-0025

homogenously hyperpolarized bioelectric pattern (in every step, except for the binary trigger, where each cell has a membrane voltage of -100 mV, at timestep zero. This was done half-way during a simulation as a loss-of-function experiment to determine whether or not they were relying on bioelectrical mechanisms for their effective morphogenetic performance. This pattern was selected because it shares no resemblance to any of the developmental bioelectric patterns used for direct and indirect pattern organisms (Figure 3B). Therefore, if an organism relied on its native bioelectric pattern for correct anatomical development, this novel pattern should disrupt that. This “Resetting Bioelectricity” experiment was modified for binary trigger organisms, as it is already a homogeneous pattern, in order to understand their temporal dependence on the binary trigger duration, to know if they are really dependent on a presentation of the binary trigger to activate the downstream pathways to resolve the morphogenetic task. The native bioelectric trigger lasts for 20 timesteps during development. So, for each organism we reset their bioelectric pattern for 1 timestep, 2 timesteps, all the way up to 20 timesteps. Then we observed how changing the duration of the binary trigger affected fitness (Supplemental Material, Figure S3).

We found that resetting bioelectricity inhibited correct development, but the impact varies with the different types of pattern. Indeed, by comparing reset scores between direct and indirect organisms, the direct organisms have population scores of 0 ( $\sigma=0$ ) while indirect organisms don't fail completely on the morphogenetic task: they have higher scores but still low in terms of development and with a lot of variance (population fitness score of 31 ( $\sigma=24\%$ ) for “Half and Half” pattern, 51 ( $\sigma=16\%$ ) for “Cross”, 48 ( $\sigma=15\%$ ) for “Triangles and 52 ( $\sigma=17\%$ ) for “LL” (Table 1). The high variance in resetting scores for indirect organisms supports the fact that different indirect organisms have different levels of dependence on bioelectricity for morphogenesis. Therefore, organisms with the direct patterns (Figure 5D) are fully dependent on bioelectricity for survival, but indirect types have less dependence.

We also found that binary trigger organisms varied in their bioelectrical dependence (see Figure 5F and Supplemental Material, Figure S3B-C). Some required only 1 timestep of their binary trigger in order to reach a fitness comparable to if they had the full 20 timestep trigger. For others, 5, 10, or 15 timesteps is necessary. Some did not require the bioelectric pattern at all to reach the target morphology. This is shown in Figure S3A, where resetting the whole binary trigger does not affect 60% of the organisms, while the rest either die or develop incorrectly. At the population level, when removing the entire binary trigger (all 20

timesteps) the fitness is on average of 58 ( $\sigma=27\%$ ). This demonstrates how resetting the full binary trigger can severely inhibit the ability for binary trigger organisms to resolve the French Flag but the high variance shows too that some organisms in the population don't rely fully on it to resolve the morphogenetic task (Table 1). The distribution of fitness scores for binary trigger organisms undergoing full resetting (Figure 5F) shows a bimodal distribution. The majority of the population didn't survive the resetting of the pattern, while the others can reach up to fitness=80, showing a low dependency on the bioelectrical pattern. Indeed, we consider that achieving less than 80/90% of the anatomy leads to unsurvivable “birth defects” (death), we set this high threshold to match the high fidelity of biological morphogenesis.

Direct, indirect, and binary trigger pattern organism examples shown in Figure 6A, 6B, and 6C, respectively, achieved fitness of 0 ( $\sigma=0\%$ ), 61.4 ( $\sigma=3.84\%$ ), and 43.6 ( $\sigma=2.29\%$ ) over 20 runs after resetting bioelectricity. Given that these specific organisms have baseline fitness of 98, 83%, and 76% without any perturbation, respectively, these organisms rely on their native bioelectric patterns for development. Generally, what occurs for these types of organisms that have their native patterns reset is the following. First, they show rapid cellular differentiation. This is what is seen in practice – cell collectives typically undergo global, rapid, and stochastic cellular differentiation. Since cellular differentiation has a metabolic cost in our model, this accelerates the demise of the organism in a positive feedback loop.

The mapping between indirect and binary trigger patterns with their downstream morphologies is complex, as opposed to the linear mapping of direct organisms. As shown in the population statistics of indirect and binary trigger organisms, some organisms with non-linear goal-encoded bioelectrical pattern (indirect and binary trigger) learn to rely less on their membrane voltages for development and may rely on other things, like local information or the starting state

TMBMC-TPS-25-0025

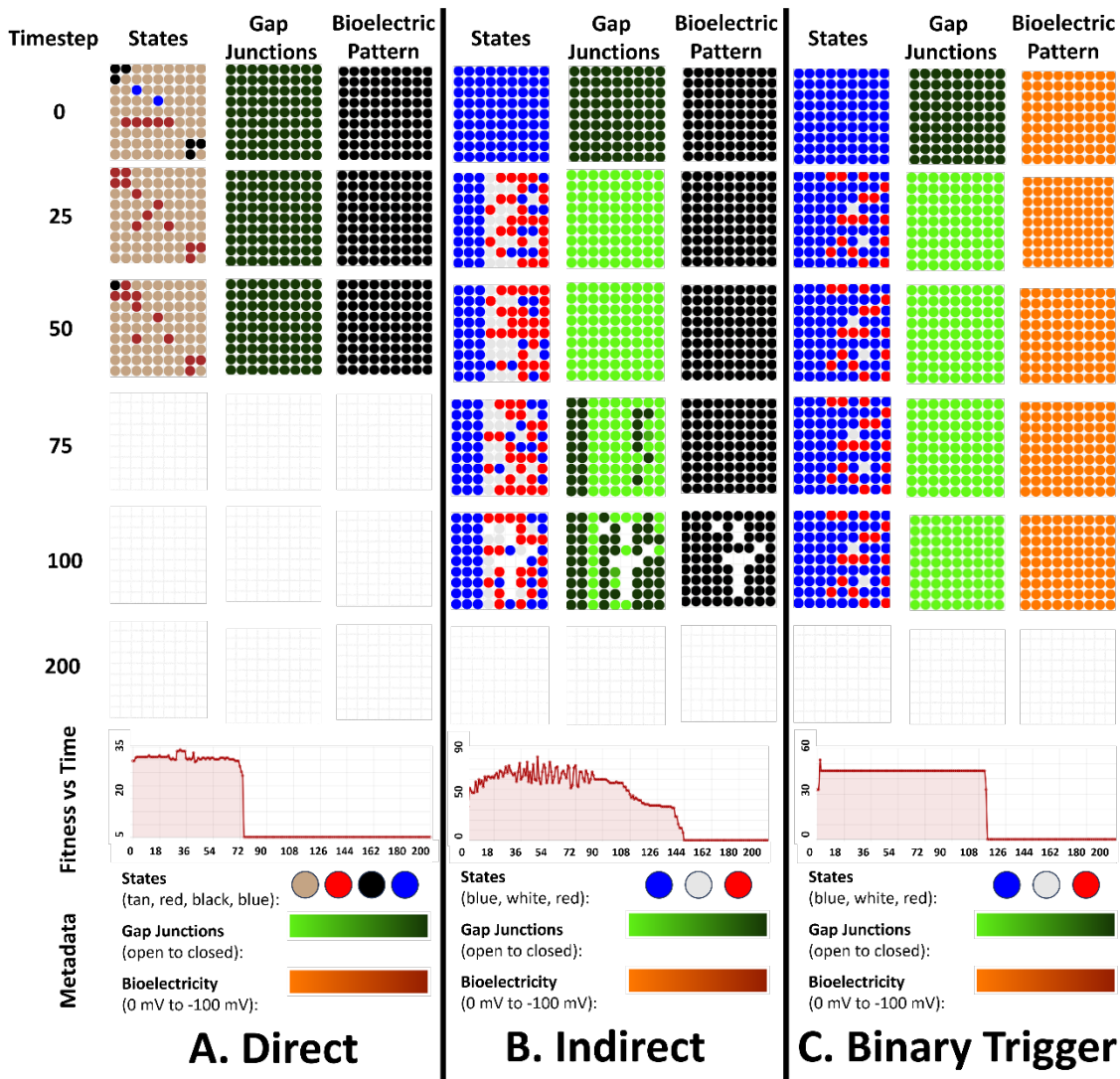


**Figure 6. Morphogenetic behavior depends on the bioelectrical patterns and the duration of the binary trigger (Resetting experiment).** Shown for each category are the temporal dynamics of cell states, molecules, and gap junctions used across 200 timesteps, sampled at six timesteps ( $T=0, 25, 50, 75, 100$ , and  $200$ ). Under that are the corresponding fitness vs. timestep chart. Finally, under that is the scales for states, molecules, gap junctions, and bioelectricity. A, B, and C are examples that show a single example for each Direct, Indirect, and Binary Trigger organismal development under the “Resetting Bioelectricity” experiment. A) Direct pattern organism example. After resetting the bioelectric pattern, the organism dies at timestep 76 due to its inability to perform anatomical homeostasis. Throughout development, cells continuously and stochastically differentiate without forming useful structures - degradation. (B) Indirect pattern organism example. After resetting the bioelectric pattern, the organism dies around timestep 69 due to its inability to perform anatomical homeostasis. Cells continuously and stochastically differentiate without forming useful structures. By step 90, fitness decreases as the organism slowly dies. C) Binary trigger organism example. The entire 20 timestep binary trigger was reset. The organism stayed in the shown configuration inadequate for survival for nearly its entire lifespan, which ended around timestep 118.

of the tissue, or a memory of the goal encoded in the neural networks of the cells.

TMBMC-TPS-25-0025

Therefore, we conclude that organisms with direct patterns are fully dependent on the bioelectric pattern (they perished immediately upon removal),

while those with indirect patterns and binary triggers can evolve to different degrees of robustness to loss of bioelectrical information, to differing extents based on

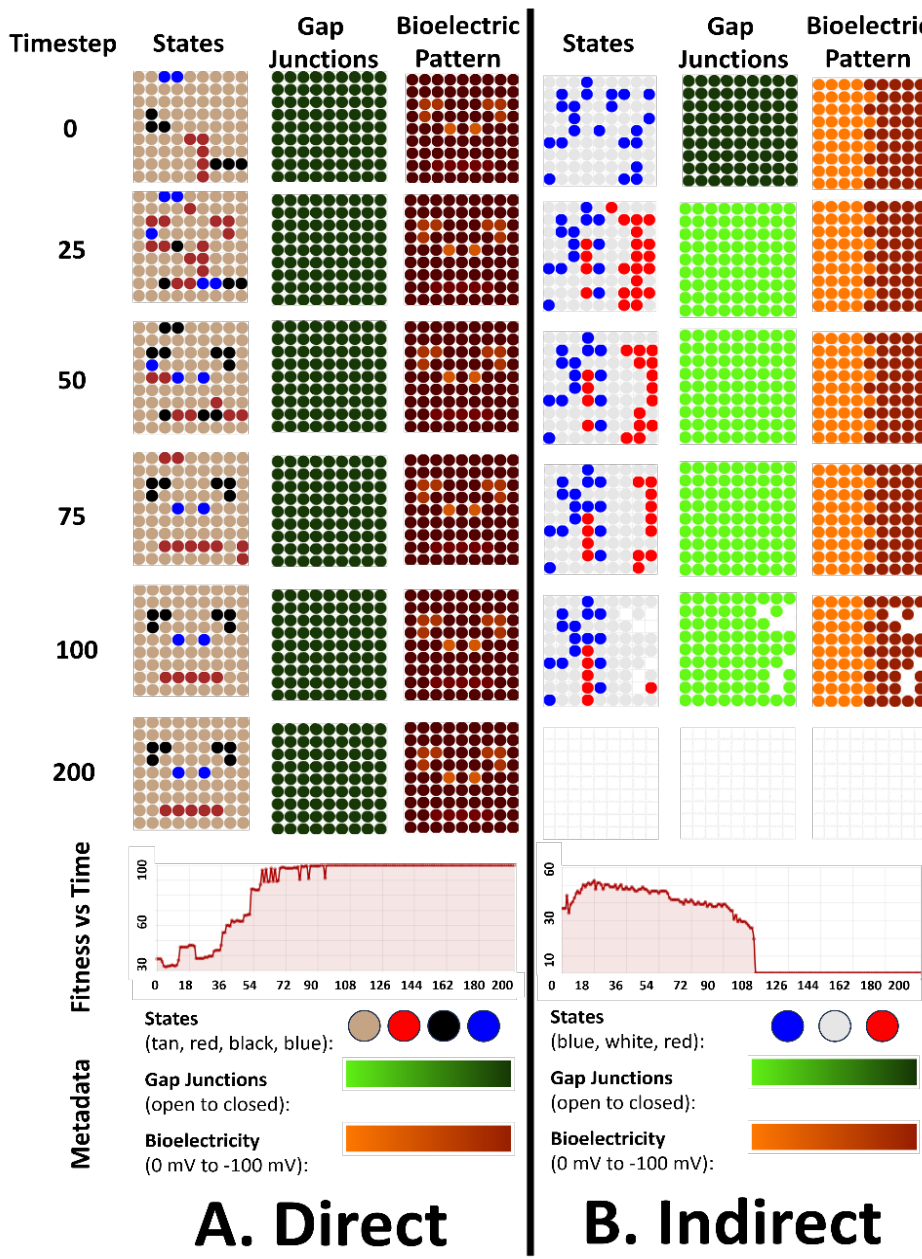


**Figure 7. An emergent morphological robustness for the direct pattern (Morphological Robustness Experiment).** Shown for each category are the temporal dynamics of cell states, molecules, and gap junctions used across 200 timesteps, sampled at six timesteps ( $T=0, 25, 50, 75, 100$ , and  $200$ ). Under that are the corresponding fitness vs. timestep chart. Finally, under that is the scales for states, molecules, gap junctions, and bioelectricity. A and B are examples that show a single successful example for each Direct and Indirect organismal development under the “Morphological Robustness” experiment. A) Direct pattern organism example. Notice that the starting morphology is scrambled compared to the normal starting condition. After scrambling the starting morphology, the organism reaches a fitness of 100 (without scrambling it reaches a fitness of 98) Activity follows the same trend as in Figure 4A. By step 100, the target morphology is completely resolved. The morphology is maintained until time 200. B) Indirect pattern organism example. After scrambling the starting morphology, the organism reaches a fitness of 31.7 (without scrambling it reaches a fitness of 87). Activity is high in the early stages of development when fitness is low, and error is high. Fitness peaks around 60 at time 25, but then gradually decreases as morphological degradation occurs.

the specific pattern and the duration of the binary trigger.

### C. An emergent robustness to changes in initial configurations for the direct pattern

Previously we showed that artificial organisms rely on bioelectricity to reach their morphogenetic setpoints (to various degrees depending on their type of bioelectric pattern) but how robust are these developmental processes to external perturbations? Indeed, did organisms learn to map the native bioelectric pattern to the target morphology, so that they may reach it from various initial states? Do they show developmental robustness[135-137]?

To address this question, we devised the “Morphological Robustness” experiment (Supplementary Material, Figure S4), in which embryos were tasked with developing into the correct target morphology despite starting off in different morphological states. We created 20 new starting morphologies for each organism (Supplementary Material, Figure S5) with direct and indirect bioelectrical patterns. Each organism was evaluated on these 20 developmental cycles for their morphological robustness. We didn’t apply this experiment to the organisms with a binary trigger as we want to understand the mapping between the goal-encoded bioelectrical pattern and the morphological initial condition, and the binary trigger is more a higher level bioelectrically encoded switch activating the memory of the cellular network to reach a specific morphology.

We discovered that at the population level, the direct pattern organisms were morphologically robust, by reaching 65 ( $\sigma=16\%$ ) of fitness score on average, with the 20 new starting morphologies (Table 1). We also observed that several organisms even reached more than 90 of fitness score after perturbation (Figure 5G). The representative example of the organism with direct pattern (see Figure 7A) scored a fitness of 97.7 ( $\sigma=3.00\%$ ) over 20 runs. The target morphology was almost complete by time 75, which is 25 timesteps earlier than the baseline (Figure 4A). The common process by which the organisms reach the anatomical setpoint from a new starting point is identical to the framework laid out in (Section 3.1).

Indirect organisms were not morphologically robust (Figure 5H), reaching at population level a fitness score of 20 ( $\sigma=12\%$ ) for “Half and Half” indirect pattern, 6 ( $\sigma=11\%$ ) for “Cross”, 2 ( $\sigma=4\%$ ) for “Triangles” and 1 ( $\sigma=2\%$ ) for “LL” for a general average of 7.25 of fitness score for organisms with indirect pattern (Table 1). The representative example of the indirect pattern organisms, utilizing the “Half and Half” pattern and a starting morphology biased towards white and blue cells, achieved a fitness of 31.7

( $\sigma=7.72\%$ ) over 20 runs (Figure 7B). By around timestep 25, the organism reached its peak fitness level and the morphology remained mostly unchanged until death. No coherent stripe was formed. Activity ceased and the organism died after timestep 110.

Thus, we conclude that direct pattern organisms show emergent morphological robustness during development to external morphological reconfiguration as a byproduct of their linear mappings between voltage patterning and target anatomy. Indirect pattern organisms displayed almost non-existent morphological robustness to changes in initial states configurations in our experiment.

### D. Emergent robustness for the organisms with indirect patterns to bioelectrical perturbation

We investigated earlier how completely resetting the bioelectric pattern inhibits correct development of the organisms with direct patterns and with different extent with organisms with indirect pattern. Would it be possible that organisms rely only on specific part of the indirect bioelectrical pattern? What about smaller perturbation, such as resetting half of the pattern or adding artificial noise to the whole pattern? To address this question, we devised the “Bioelectric Robustness” experiments (Supplementary Material, Figure S6). We focused this experiment solely on organisms with indirect patterns, due to their lack of morphological robustness and the possibility that the key to their robustness lies in the nonlinear dependencies they learned from their bioelectric patterns. Also, the direct bioelectrical pattern encodes a direct mapping with the goal to reach in the morphospace and would not be expected to be robust to its alteration.

We evaluated the resilience of the indirect pattern organisms to bioelectric perturbations by either: i) resetting half of their bioelectrical patterns (by hyperpolarizing them to -100mV, similar to section 3.2) ii) introducing noise (by polarizing cells by a random choice of -20, -10, -5, 0, 5, 10, or 20mV). Each organism was evaluated on these two developmental cycles for their bioelectric robustness.

We found that there is large variance at population level, which has “Cut” robustness fitness scores of 31 ( $\sigma=31\%$ ) for indirect pattern “Half and Half”, 42 ( $\sigma=29\%$ ) for “Cross”, 43 ( $\sigma=32\%$ ) for “Triangles” and 40 ( $\sigma=32\%$ ) for “LL” for an average fitness of 39 of fitness score for organisms with indirect pattern (Table 1). “Noise” population robustness fitness scores also had high variance, with a score of 47 ( $\sigma=26\%$ ) for “Half and Half”, 43 ( $\sigma=24\%$ ) for “Cross”, 41 ( $\sigma=27\%$ ) for “Triangles”, and 44 ( $\sigma=27\%$ ) for “LL” for an average fitness of 43.75. It appears that, the population of indirect organisms display a bimodal distribution for fitness scores under the “Cut” and

TMBMC-TPS-25-0025

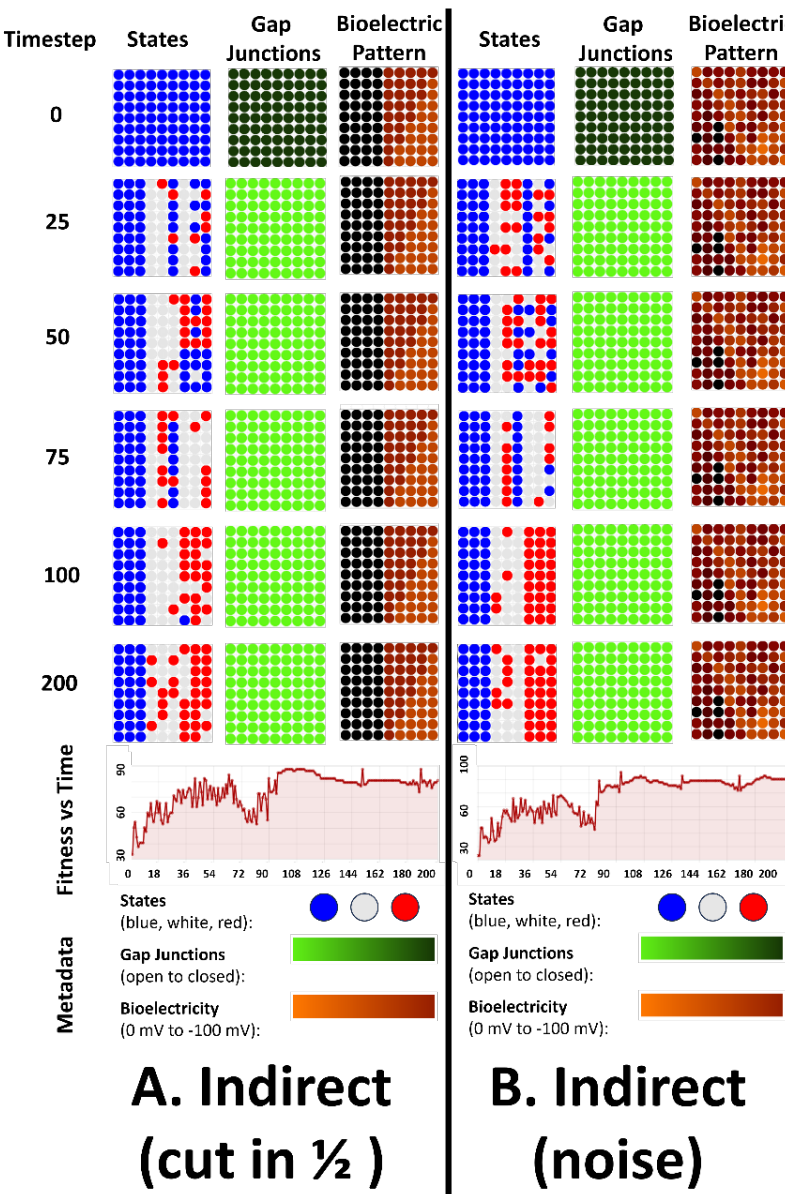


**Figure 8. Relative bioelectric robustness for the organisms with indirect patterns to bioelectrical perturbation (Bioelectric Robustness Experiment).** Shown for each category are the temporal dynamics of cell states, molecules, and gap junctions used across 200 timesteps, sampled at six timesteps ( $T=0, 25, 50, 75, 100$ , and  $200$ ). Under that are the corresponding fitness vs. timestep chart. Finally, under that is the scales for states, molecules, gap junctions, and bioelectricity. A, and B are examples that show a single example for each Indirect (cut in half) and Indirect (noise) organismal development under the “Bioelectric Robustness” experiment A) Indirect pattern organism for the “cut” bioelectrical robustness experiment. After cutting the bioelectric pattern, the organism reaches a fitness of 89 (without cutting it reaches a fitness of 92). By step 100, activity has ceased and fitness declines. The red stripe is incomplete, and the white stripe has a few extra red cells. B) Indirect pattern organism for the “nose” bioelectrical robustness experiment. After introducing noise in the bioelectrical pattern, the organism reaches a maximum fitness of 96 (without noise it reaches a maximum fitness of 96). By step 100, activity has ceased and fitness plateaus. The target morphology is legible, and the white stripe has a few extra red cells. The tissue maintains its state well until timestep 200.

“Noise” robustness experiments (Figure 5I and Figure 5J). We have two groups in each condition, one composed of organisms that didn’t survive the bioelectrical perturbation and another that presented emergent robustness during evolution.

The representative example of the survival group of the organisms with the “Triangles” indirect pattern (Figure 8B) achieved a fitness of 82.9 ( $\sigma=7.16\%$ ) and a fitness of 84.4 ( $\sigma=6.89\%$ ) over 20 runs for the cut and noise experiments, respectively. “Half and Half” organisms outperformed other indirect populations in

TMBMC-TPS-25-0025

Noise Robustness, but underperformed in Cut Robustness. The former may be due to the relatively low structural complexity of “Half and Half” compared to the other indirect patterns. The latter is easy to understand, because the “Half and Half” contains half of its information on each side, since both left and right halves have different polarization levels. Therefore, we conclude that indirect bioelectric patterns have emergent robustness to bioelectric perturbations during development.

#### E. An emergent generalizability competency to new bioelectrical pattern for the direct and indirect pattern organisms.

Animals can be anatomically altered by reprogramming their developmental bioelectric software[14], such as: regenerating planaria induced to grow two heads or no heads [29] or heads of other species[27,67], or *X. laevis* developing functional ectopic eyes in aberrant locations[138]. We wanted to know if we could reprogram organisms to reach new target morphologies by simply changing their native bioelectric pattern at initialization. Can they generalize past the relationship between their native bioelectrical pattern and target morphologies?

To answer that question, we devised the “Generalizability” experiment (Supplementary Material, Figure S7). For each organism, we created 3 new bioelectric patterns by rotating their native pattern by 90°, 180°, and 270° (relative to their initial orientation). Each organism was initialized with these novel patterns after they have been evolved with the standard parameters and patterns and then evaluated for their generalizability.

At the population level, direct pattern organisms reached a fitness score of 83 ( $\sigma=9\%$ ). While indirect organisms were less successful with generalization, they reached at population level a fitness score of 57 ( $\sigma=20\%$ ) for indirect pattern “Half and Half”, 27 ( $\sigma=7\%$ ) for “Cross”, 24 ( $\sigma=2\%$ ) for “Triangles” and 23 ( $\sigma=3\%$ ) for “LL” for a general average of 32.75 of fitness score for organisms with indirect pattern (Table 1). This difference in performance is also reflected in the population level shown in Figure 5K and Figure 5L. Direct organisms all survived development (Figure 5K), while there seems to be two classes of indirect organisms: those that die (the majority of the organisms) and those that are moderate to high for generalizing and are successful at development, mainly with ‘Half and Half’ pattern (Figure 5L).

The representative examples of the direct pattern organism and indirect pattern organism (utilizing a “Half and Half” pattern) shown in Figure 9A and 9B, have fitness scores of 92.8 ( $\sigma=6.93\%$ ) and of 79.4

( $\sigma=16.1\%$ ) over 20 runs, respectively. The strategy that organisms followed was almost the same as their original strategies in standard conditions.

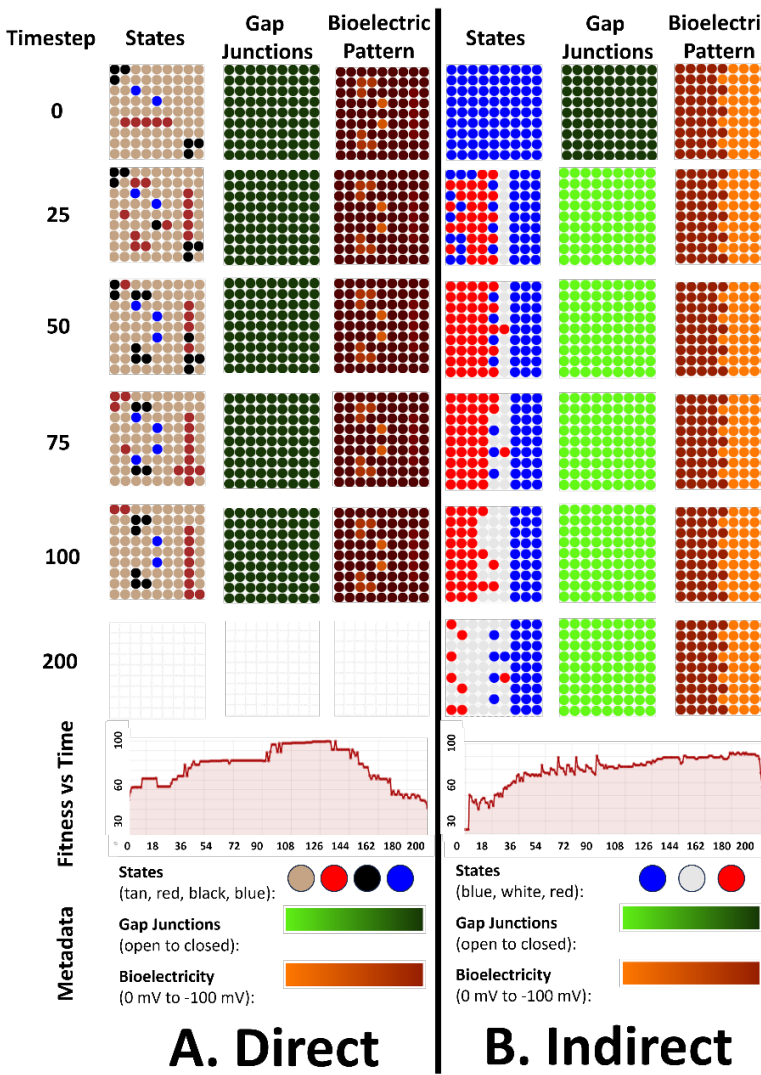
Thus, we observed that the organisms learned a larger mapping between the bioelectrical patterns and the target morphology. Through experiments comparing normal development to outcomes after bioelectric pattern rotation, we found that organisms with direct and indirect bioelectrical patterns adapted well and show emergent generalizability competency to new bioelectrical patterns.

#### F. An emergent repatterning capabilities for direct pattern organisms in post-developmental phase.

We showed in the previous section that artificial embryos could be reprogrammed to generalize to novel target morphologies that had never been learned in their developmental cycles. A similar biological phenomenon involving morphological remodeling is that of repatterning[139]. This involves the reorganization and reconfiguring of biological tissue to achieve a new outcome, such as the remodeling of adult epibranchials of metamorphosing species of lungless salamanders during development [140] or wound healing and blastema formation during *Drosophila* larvae imaginal disk regeneration[141]. In the context of our simulation, we define repatterning as the ability for an organism, after the conclusion of its 100 timestep developmental period, to remodel its cells to reach a new morphological state given a novel bioelectric pattern. Previous work [97] showed that artificial organisms are capable of morphological allostasis in this post-developmental period. This ability to maintain anatomical stability with dynamic responses after development was not directly programmed in by the modeler and is therefore emergent. If artificial organisms during the post-developmental period have the emergent ability to fitness distributions for generalizability, maintain their form, do they also have the emergent ability to create new forms (repatterning)? Can we induce them to repattern themselves into new morphologies by only changing their bioelectric patterns during the developmental phase?

To answer that question, we devised the “Repatterning” experiment for direct and indirect patterns organisms (Supplementary Material, Figure S8). This experiment is identical to the “Generalizability” experiment (Section 3.4) except each organism was allowed to develop normally until timestep 100 when these novel patterns replaced the native ones. The energy levels for these organisms were reset back to maximum at the start of the

TMBMC-TPS-25-0025



## A. Direct      B. Indirect

**Figure 9. The organisms learned a mapping between the bioelectrical patterns and the target morphology (Generalizability Experiment).** Shown for each category are the temporal dynamics of cell states, molecules, and gap junctions used across 200 timesteps, sampled at six timesteps ( $T=0, 25, 50, 75, 100$ , and  $200$ ). Under that are the corresponding fitness vs. timestep chart. Finally, under that is the scales for states, molecules, gap junctions, and bioelectricity. A) Direct pattern example. After rotating the bioelectric pattern, the organism reaches a maximum fitness of 96 (without rotation it reaches a fitness of 98). Activity follows the same trend as in Figure 4A. By step 100, the target morphology is completely resolved. Then begins the gradual degradation of the target morphology until the organism dies at time 185. The target morphology looks close to the expectation – the original target morphology rotated 90 degrees counter-clockwise. B) Indirect pattern example. The indirect bioelectric pattern has also been rotated at  $T=0$ , this time by 180 degrees. After rotating the bioelectric pattern, the organism reaches a maximum fitness of 90 (without rotation it reaches a fitness of 90). The target morphology looks close to the expectation – the original target morphology rotated by 180 degrees.

repatterning period as for most of the organisms were exhausted after development. They were then evaluated at timestep 200 for their repatterning ability.

We found that at populations level, for direct bioelectrical pattern organisms, their fitness was 22% ( $\sigma=33\%$ ), a stark drop from the 83 ( $\sigma=9\%$ ) population average for generalizability (Table 1). The high variance in outcomes for organisms repatterning means that some organisms start to repattern, while

others cannot. Indirect organisms also had low repatterning capabilities, with an average fitness of 13 ( $\sigma=14\%$ ) for the entire population of Half/Half indirect pattern organisms, 7 ( $\sigma=11\%$ ) for “Cross”, 1 ( $\sigma=3\%$ ) for “Triangles” and 0 ( $\sigma=0\%$ ) for “LL” for an general average of 5.25 of fitness score for all the organisms with indirect pattern (Table 1). Looking at the population level fitness histograms, we found that even if the entire direct pattern population tended to

TMBMC-TPS-25-0025

have low fitness scores, they contained a few organisms that showed some level of competency at repatterning (as displayed in the histogram, Figure 5M), such as in Figure 10A. However, overall, indirect

organisms performed poorly with no organisms that can reach a fitness score over 50 after 100 steps, meaning a 0% survival rate (Figure 5N).

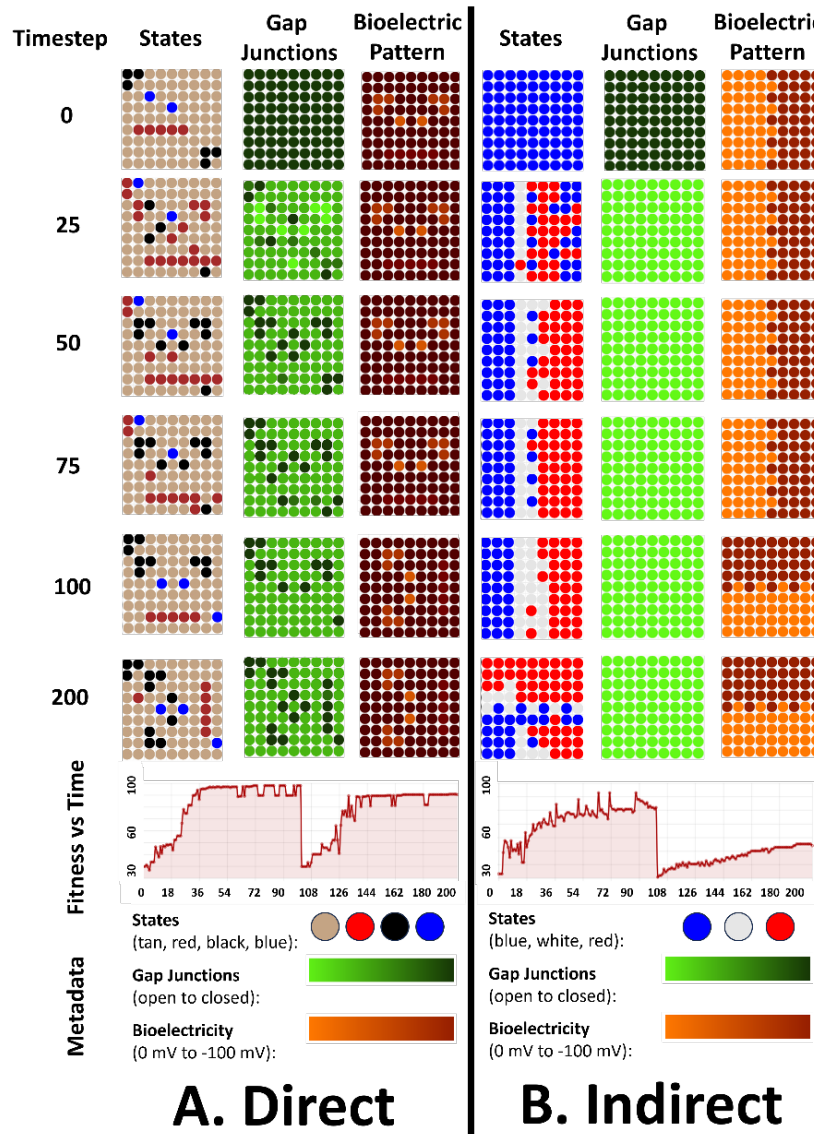


**Figure 10. Emergent repatterning competency for the direct pattern organisms in post-developmental phase (Repatterning experiment).** Shown for each category are the temporal dynamics of cell states, molecules, and gap junctions used across 200 timesteps, sampled at six timesteps ( $T=0, 25, 50, 75, 100$ , and  $200$ ). Under that are the corresponding fitness vs. timestep chart. Finally, under that is the scales for states, molecules, gap junctions, and bioelectricity A) Direct pattern organism example. After rotating the bioelectric pattern 90 degrees counterclockwise at timestep 100, the organism reaches a maximum fitness of 91 at time 200 (without rotation it reaches a fitness of 99 at 200). This is not the organism shown as the one in Figure 2, as the previous organism could not perform repatterning, but this one could. For this organism, its gap junction openings are highly correlated with cell type. At 100 the upright morphology is complete, but the new rotated target morphology and bioelectric pattern are introduced. Consequently, fitness sharply plummets but activity stays constant. The target state at timestep 200 has a fitness of 91, close to the desired rotated target state. B) Indirect pattern organism example. After rotating the bioelectric pattern (top-right arrow), the organism reaches a fitness of 92 (without cutting it reaches a fitness of 92). At 100 the French Flag is complete, but the new rotated target morphology and bioelectric pattern are introduced. Consequently, activity increases, and fitness sharply plummets. The target state at timestep 200 has a fitness of 55, it is more than halfway there to reaching the rotated target state.

TMBMC-TPS-25-0025

We observed that successful repatterning ability for direct pattern organisms follow the general behavior of previous experiments with direct pattern organisms typically more capable than the indirect pattern ones. The direct pattern organism and indirect pattern organism (utilizing a “Half and Half” pattern) examples are shown in Figure 10A and 10B, scoring a 200-timestep fitness of 83.0 ( $\sigma=7.02\%$ ) and of 54.3 ( $\sigma=2.96\%$ ) over 20 runs, respectively. Both patterns are rotated 90 degrees counterclockwise at time 100, and fitness was now evaluated at time 200 instead of 100.

Thus, we can conclude that artificial organisms with direct patterns have the emergent ability to repattern themselves after evolutionary training and alter their adult morphology in response to a changed bioelectric pattern. Conversely, those with indirect patterns don’t exhibit any repatterning capability (Figure 5N).

## V. SELECTIVE SEROTONIN REUPTAKE INHIBITORS (SSRI) SIMULATION AND EXPERIMENTAL RESULTS

Selective serotonin reuptake inhibitors (SSRIs) are a class of drugs prescribed for cases of depression and anxiety[142-145]. They mainly target a component of the serotonin signaling system, the serotonin transporter, SERT. Serotonin signaling has previously been implicated as a component of bioelectric circuits[142]. Some have suggested that SSRIs target bioelectricity in the context of developmental defects[142,146,147]. SSRIs act on the serotonin signaling system, which has been suggested to be involved in processing rewards and punishments in the brain[148,149]. SSRIs can also function to change membrane voltage of neural and non-neural cells [142,150,151].

As found above, artificial organisms learned a mapping between target morphology and their native bioelectric pattern that is robust and amenable to generalization and repatterning. Does that mapping start to break down under the influence of SSRI-like conditions? Does that lead to morphological defects in artificial organisms as seen in biological organisms[147]? To answer these questions, we simulated SSRI exposure by altering the reward system in our model. We changed their cellular reward machinery by eliminating the energy increment/reward at each step similarly to SSRI exposure as shown in [148,149] where serotonin plays a pivotal role in reward processing to explore its effects on the development of artificial organisms and made predictions we verified experimentally.

### A. Simulated SSRI induced loss of regenerative precision and a bistable morphogenetic process

In order to simulate an SSRI exposure experiment, we started by evolving organisms that would pursue the French Flag morphology with an indirect pattern. To model SSRI, we have chosen a homogeneously depolarized bioelectric pattern that we selectively perturbed bioelectrically (as shown in Figure 11). This new pattern resembles the “Rest” pattern shown for binary trigger organisms (Figure 3B). Even so, these organisms are not binary trigger organisms because they are only exposed to one pattern for their entire developmental period (as opposed to binary trigger organisms which alternate between two patterns).

Next, we selected 20 of these organisms that showed dependency on bioelectricity (Section 3.2) and that had a fitness of 90 or more on the given task. At the population level, the fitness for this group was 92.4 ( $\sigma=2.1\%$ ) (Supplemental Material, Figure S9A). Then, we altered their cellular reward machinery by eliminating energy increment (which is a reward in our system) at each step and by perturbing bioelectrical states similarly to SSRI exposure [148,149][150,151]. Thus, cells may no longer gain top-down instructive information on morphological error. We perturbed the voltage of 1, 2, 5, and 10 random cells at once, by hyperpolarizing them anywhere from -5, -10, or -30 mV.

This simulated experiment led to two discoveries: global morphological degradation and a bistable development. Global morphological degradation, in a biological context, can be thought of as the inability for a cellular collective to determine how to differentiate to reach the target morphology. This state is characterized by a significant deviation from the target morphology and frequent random, undirected differentiation of the cells, or a loss of precision in organisms’ normally quite tight ability to reach the same, invariant pattern. Multistability in dynamical systems theory is “the ability of a system to achieve multiple steady states under the same external conditions”[152]. In a developmental biology context, this would equate to an organism that can become one of multiple target anatomies, under the same environment. There are many animals that exhibit this behavior under different contexts, such as planaria during regeneration[64].

#### 1. SSRI exposure leads to global morphological.

TMBMC-TPS-25-0025

By simulating SSRI exposure as defined above with the alteration of the cellular reward mechanisms (via removing energy reward) and bioelectric states (via randomized voltage perturbations of cells), we found that the number of cellular voltage perturbations was the key factor that determined whether global morphological degradation (loss of morphogenetic precision) occurred or not (Figure 11). Hyperpolarizing only one cell did little to affect development. However, hyperpolarizing two cells was enough to begin to see a disruption of anatomical homeostasis. Development would typically proceed along a similar trajectory as normal, however there

would be a slight increase in rapid “back-and-forth” cellular differentiations. Sometimes, the target morphology would be worse due to misplaced cells and incomplete structures. Moreover, the global morphological degradation became most apparent when five or more perturbations were introduced to the SSRI-exposed organism. Depending on their placement, a general weakening of anatomical homeostasis could occur (Figure 11C), or the birth of a bistable developmental process (Figure 11B).

A factor that impacted the occurrence of global morphological degradation was the location of perturbations. As discussed in depth in the next

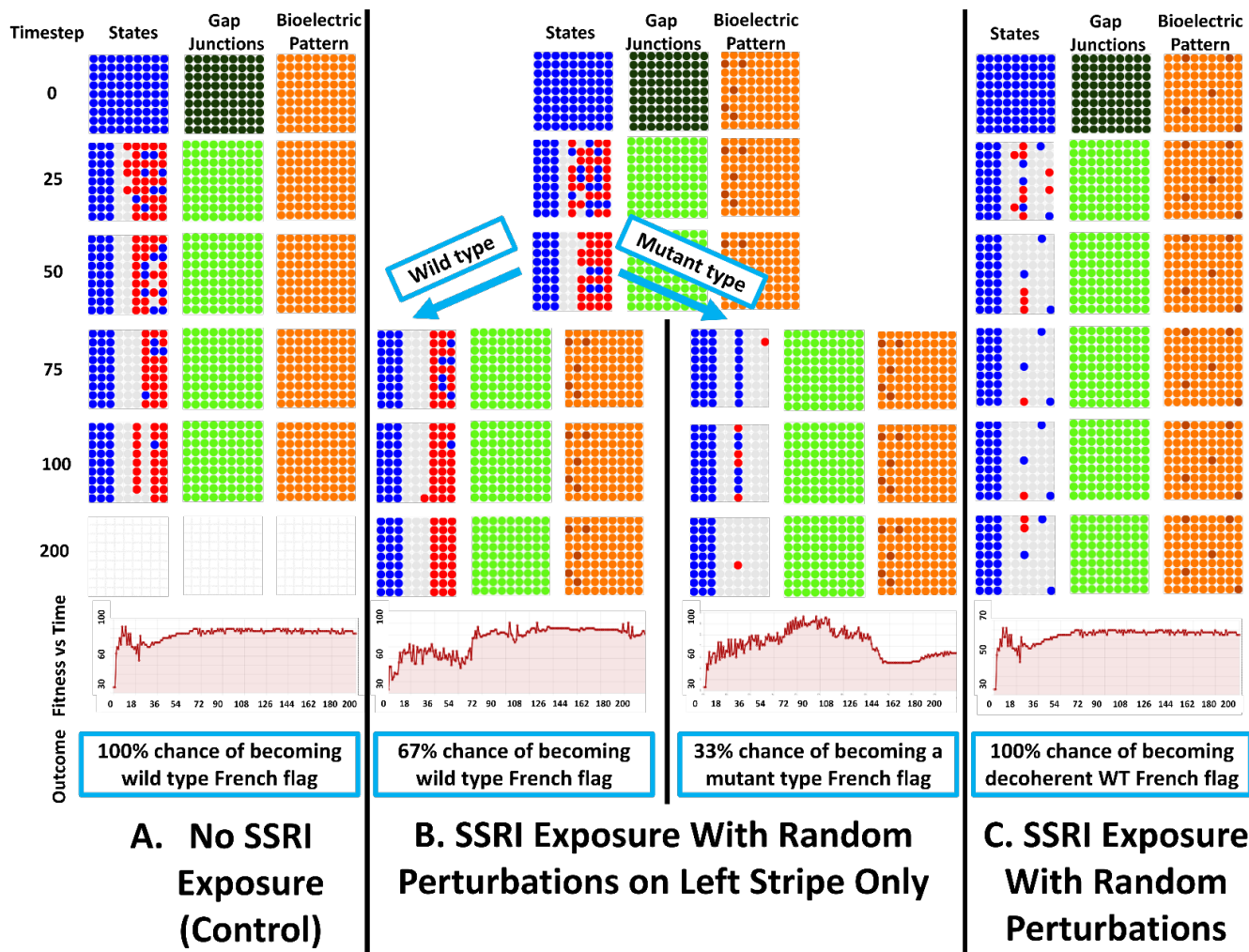


**Figure 11. SSRI exposure leads to a bistable development process.** To see if SSRI exposure causes monostable organisms to become bistable or multistable and pursue multiple developmental attractor states, we simulated SSRI exposure on French Flag organisms with homogeneously depolarized patterns and perturbed the bioelectric pattern of several cells at once (A) No SSRI exposure. The organism reaches the wild type French Flag target morphology, 100% of the time. In this instance, there is some error on the white and red stripes but the French flag is still visible. (B) SSRI exposure with random perturbations on the left stripe. Applying SSRI exposure to the same organism (via changing the reward machinery) and perturbing 5 random cells from the left stripe of the organism by hyperpolarization of -30 mV causes a bistable developmental process to occur. This causes there to be a 67% chance of forming the wild type morphology (with higher resolution, likely due to the removal of energy loss) and a 33% chance of forming a new, mutant type morphology. This was measured over 100 runs. (C) SSRI exposure with random perturbations. Adding 5 more -30 mV perturbations to the same SSRI exposed organism, except no longer localized to the left stripe, causes global morphological degradation and a return to a unistable developmental process. The fully resolved French flag is no longer apparent – instead the red stripe is replaced by a white stripe with blue and red cells scattered. During the simulation, there are rapid cellular differentiations indicative of degradation.

TMBMC-TPS-25-0025

section, on rare occasions the specific cells that become hyperpolarized can be the difference between a benign perturbation that has seemingly no effect on morphogenesis, and an alternate developmental pathway. That factor usually impacts degradation in concert with another factor, the order of cellular activations during development. Interestingly, an insignificant factor was the magnitude of the cellular hyperpolarizations. For any given organism, hyperpolarizing an identical set of cells by -5, -10, or -30 mV had no distinguishably different effect. This could be because the organism and its ancestors were only exposed to one voltage value (0 mV) throughout their lifecycles, thus they never learned to distinguish between different voltage states.

Based off these observations, we designed a test to quantify morphological degradation by comparing the fitness of these 20 organisms before and after SSRI exposure with perturbations (Supplemental Material, Figure S9). In this experiment, we exposed each organism to SSRI and perturbed 5 random cells, as described above. We did this three times for each organism and averaged the fitness values to get a mean fitness score for each organism. At the population level, the fitness for these organisms dropped from 92.4 ( $\sigma=2.1\%$ ) to 54.8 ( $\sigma=13.3\%$ ) (Supplemental Material, Figure S9).

By altering cellular reward mechanisms (via removing energy loss) and bioelectric states (via randomized voltage perturbations of cells) similarly to SSRI exposure, we induced widespread morphological degradation in our model organisms similarly to results reported in biological experiments[147].

## 2. SSRI exposure leads to a bistable developmental process.

We also found that SSRI simulated exposure leads to leads to a multistable developmental process in a one representative organism (Figure 11). Under normal conditions, this organism reaches the French Flag morphology with a fitness of 74.5 ( $\sigma=15.1\%$ ), as shown in Figure 21A. When this organism was subjected to random perturbations of 1 cell at a time, no notable degradation or change in stability ever occurred. When multiple cells were perturbed at random, there was noticeable degradation but no multistability. However, we observed that when only the cells of the left stripe were perturbed, regardless of the amount of hyperpolarization for each cell or the number of cells that were hyperpolarized, the organism exhibited a bistable developmental process. Over 100 runs on the configuration shown in 10B, this organism had a 67% probability of developing into the wild type expected morphology, with the remaining

33% of times resulting in an entirely distinct form (Figure 11B). In this bistable mode, the organism had a fitness of 91.4 ( $\sigma=11.5\%$ ). Interestingly, when it solved the French Flag it always did so with near perfection, getting 98-100 fitness. When it pursued the mutant type morphology, the fitness was closer to 55-66. This new mutant type of morphology had no red stripe, a central 1-cell thick blue and red stripe at time 100, and a central red dot or dots at time 200 that replaced the blue stripe.

This bistable phenomenon quickly disappeared as soon as a cell was perturbed outside of the left stripe area (Figure 11C). Once again, the number of perturbations and degree of hyperpolarization does not matter – as soon as a cell outside of the blue stripe is perturbed on the bioelectrical pattern, there is morphological degradation. This leads to a French flag-like morphology, except it is typically missing its red stripe and with many actively differentiating cells in the red stripe area (Figure 11C). The fitness dropped to 63.6 ( $\sigma=0.82\%$ ) when perturbing outside of the left stripe. As indicated by the small deviation, this effect reliably reproduced the same morphologically decoherent morphology shown in Figure 11C.

We can conclude that this bistable phenomenon indicates that SSRI-like exposure paired with specific bioelectric modifications can induce a bifurcation in developmental pathways, leading to alternative stable morphologies. This connects to work done in tadpoles showing how depolarization of as little as three cells could cause an alternate, large-scale developmental pathway to emerge[153]. The complexity of bioelectric influences on development suggests that SSRI exposure by disrupting the top-down information related to the developmental reward may unlock latent developmental trajectories, resulting in divergent morphological outcomes under identical conditions. This finding is surprising as changing only a few cells via induced hyperpolarization causes a multi-stable developmental trajectory to emerge. Therefore, we decided to test experimentally this prediction.

## B. SSRI experimental results: regenerating planaria in fluoxetine or sertraline

Our model made a prediction about the loss of morphogenetic precision resulting from loss of stress-induced motivation driving the anatomical homeostatic loop. We sought to test this *in vivo*, using a widely available class of drugs that are used for reducing anxiety in humans and other animals [154-160] and that has previously been tested in planaria in toxicology [161,162] and parasitology [163] contexts:

TMBMC-TPS-25-0025

the serotonin reuptake inhibitors Fluoxetine and Sertraline. Specifically, these SSRIs have been studied with respect to their effects on reducing behavioral motivation and the drive for specific outcomes[164-166], similarly to the computational implementation shown above. In other words, SSRIs can alter the reward system in the organism. Applying either drug to middle fragments of planarians (Figure 12A) resulted in a mix of 0-, 1-, and 2-headed regenerates (Figure 12B, quantified in 11C). Compared to exclusively 1-headed animals in control conditions ( $n>500$ ), cohorts treated with Sertraline or Fluoxetine exhibited respectively 31% and 17% 0-headed animals, and 4% and 8% 2-headed animals ( $n=90$ ,  $n=155$  respectively). This effect was significant to  $p<0.01$  ( $2.79\times 10^{-36}$ ), from which we conclude that serotonin reuptake inhibitors reduce the precision (but do not induce one consistent anatomical fate) of regeneration.

## VI. DISCUSSION

This study utilized evolutionary simulations to explore the role of bioelectric signals in guiding morphological outcomes during development. The traversal of morphospace during embryogenesis involves a number of biophysical and biomechanical modalities. While we focused on bioelectricity in this

study, we are not claiming that bioelectric mechanisms are the only ones that can implement the dynamics we describe. Future work can examine the implications of these ideas for biochemical morphogen gradients, gene regulatory networks, biomechanics, and other signals.

The role of bioelectric patterns in morphogenesis can be classified into three types—direct encoding, indirect encoding, and binary trigger—there is a lack of computational tools to understand how these patterns evolve and confer advantages. To address these gaps, we developed a neural cellular automaton (NCA) and used evolutionary algorithms to optimize these models for reliable, regulative morphogenesis driven by the three types of bioelectric patterns. We found that: (1) All types of bioelectrical codes allow the reaching of target morphologies (2) Morphogenetic behavior depends on the bioelectrical patterns and the duration of the binary trigger (3) An emergent morphological robustness for the direct pattern (4) A relative emergent bioelectric robustness for the organisms with indirect patterns to bioelectrical perturbation (5) An emergent generalizability competency to new bioelectrical pattern for the direct and indirect patterns organisms (6) Emergent repatterning competency for the direct pattern organisms in post-developmental-phase.

Seeking to understand the dynamics of stress and reward in the guidance of anatomical error reduction

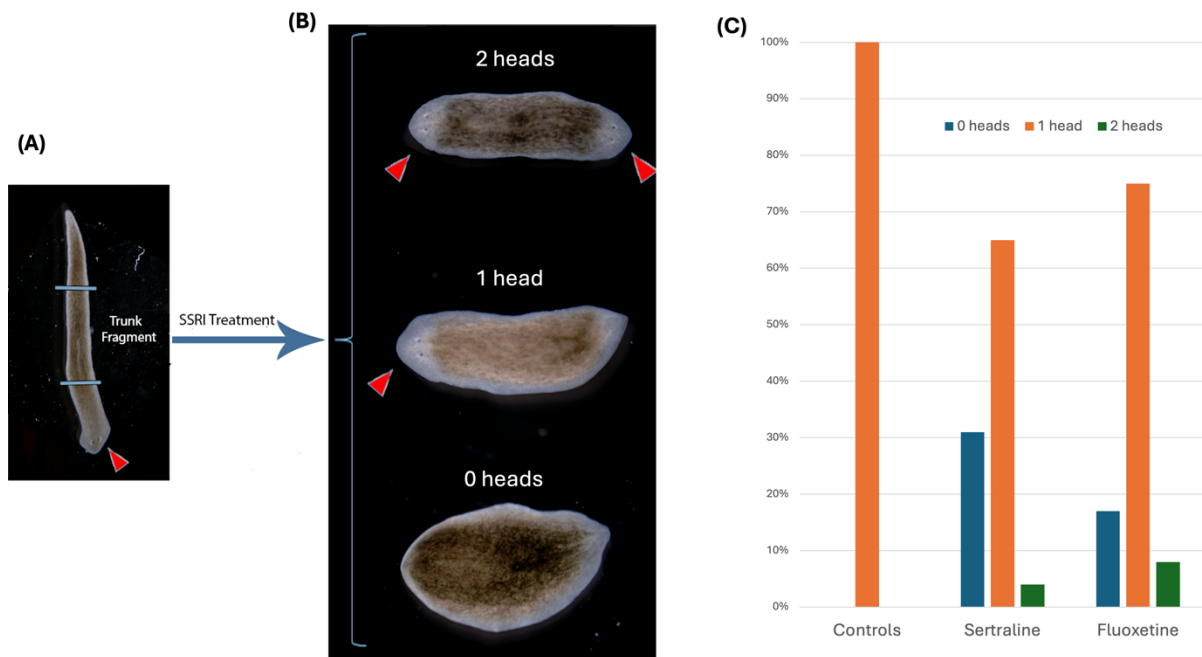


**Figure 12. Effects of SSRI on regenerative morphology in planaria.** Middle trunk fragments (A) exposed to Fluoxetine or Sertraline during the first 3 days of regeneration give rise to animals with 1-, 0-, or 2-headed anatomies (B, red arrowheads point to heads), in contrast with the extremely reliable 1-headed outcome in controls (quantification in C).

in morphogenesis, we developed a selective serotonin reuptake inhibitors simulation, which diminished the ability of artificial embryos to correctly interpret bioelectric patterns due to an altered organismal reward machinery, leading to higher variance of developmental outcomes (loss of precision), global morphological degradation, and induced in some organisms anatomical bistability. We simulated the effects of selective serotonin reuptake inhibitors (SSRIs) on artificial embryos, observing that these inhibitors impaired the correct interpretation of bioelectric patterns. These computational findings have been validated by data collected from planaria SSRI exposure. It should be noted that while the interplay between serotonin and bioelectric signaling have been studied in embryogenesis, much remains to be discovered about the ways in which neurotransmitter reward and stress-driven error minimization systems guide the interpretation of bioelectric signals toward correct target morphologies. This represents an important avenue for future work.

In the context of somatic pattern memories and bioelectric circuits underlying regeneration, electric circuits produced by ion channels are well-known to have the property of bistability in their state space, enabling a cell to be readily pushed to one of two physiological attractors[167-172]. When deployed across cell fields, such stochasticity [168,170,172-174] can induce bistability of large-scale anatomies, which has been studied using concepts borrowed from perceptual bistability in the visual system (e.g., rabbit-duck or Necker cube illusions)[64]. This stochasticity allows bioelectric networks to explore multiple potential stable states, enabling the system to stabilize in one of these configurations. This process facilitates dynamic responses in regenerative mechanisms, where cells leverage bioelectric encoding to restore anatomical structures effectively outcomes[64]. This is achieved through the exploitation of bioelectric encoding of distributed goal states, akin to how the brain utilizes memory to achieve specific outcomes[64]. The concept of bistability is not only relevant in the context of regeneration and developmental biology but also extends to neuroscience. It suggests that bistability plays a role in cognitive processes and memory formation, drawing parallels between bioelectric circuits in regeneration and neural networks involved in memory, representation, and perceptual bistability[1]. This highlights the interconnectedness of bistability across different biological systems, emphasizing its significance in understanding complex biological phenomena. Moreover, the utilization of bistability in bioelectric circuits underscores the dynamic nature of cellular processes, similarly to neural processes, where stability and

plasticity coexist to drive cellular differentiation and specialized functions in multicellular organisms[175].

We found several differences between organisms with direct and indirect bioelectrical pattern. Direct pattern organisms have a good morphological robustness to changes in the initial conditions while indirect pattern organisms in our simulation didn't develop this capability fully. However, these organisms showed an emergent robustness to bioelectric perturbations while direct pattern organisms by definition don't have this competency as the direct mapping between bioelectricity and the anatomy implies that any change in the bioelectrical pattern will result in a developmental defect. This is maybe why evolution co-opted indirect bioelectrical patterns. Indeed, organisms solely relying on direct pattern are disrupted more easily as organisms learned a direct mapping, any change in the goal-encoded bioelectrical direct pattern would lead to developmental defect, whereas indirect pattern may allow for the encoding of redundancy of the information necessary to reach the morphological goal. Evolutionarily, indirect pattern organisms may have a better fitness overall as they have such a robustness. In addition, learning an indirect mapping between morphology and an indirect bioelectrical pattern may allow the exploration of a larger morphospace than the one encoded in a direct one. It allows for more adaptability as an indirect mapping can represent more morphologies than a direct one.

Evolutionarily, organisms with indirect bioelectrical patterns likely possess greater overall fitness due to their robustness. Moreover, learning an indirect mapping between morphology and bioelectrical patterns enables the exploration of a larger morphospace compared to direct mappings. This greater adaptability stems from the ability of indirect mappings to represent a broader range of morphologies or compressed morphological information. Our simulated experimental comparisons between normal development and outcomes following bioelectric pattern rotation indicate that both direct and indirect pattern organisms adapt well and exhibit emergent generalizability to new bioelectrical patterns. This competency may facilitate the introduction of new patterns in evolution, enhancing adaptability and overall fitness.

Our model makes a specific prediction for loss-of-function targeting of motivation pathways in regenerative morphogenesis, which we decided to test *in vivo*, via the serotonergic route. The serotonin neurotransmitter system exists in planaria. An ortholog of tryptophan hydroxylase, which catalyzes the rate-limiting step in serotonin synthesis, has been identified in *D. japonica*[176], planarian serotonin receptors have also been characterized[177,178], and

several studies have found that SSRI treatment impacts planaria in numerous ways including behavior, DNA damage, and regeneration[162,163,179,180].

We found that two different serotonin reuptake inhibitors induced a “randomizing” effect in planarian regeneration, in which the normally extremely reliable regeneration of 1-headed animals from fragments was driven to sometimes produce 2-headed and sometimes 0-headed animals. This is unusual because conventional treatments, such as inhibition of the Wnt signaling pathway, typically reliably produce inhibition of head character *or* excess anteriorization[181-183].

The ability to reduce morphogenetic precision, and thus create a stochastic phenotype where both extremes are represented, instead of pushing the system into one specific direction along the anterior-posterior decision axis, is notable. That, and the fact that the phenotypes featured apparently normal heads with no tissue-level defects, are consistent with our contention that the stress-based system is regulating global information processing and error minimization, not a specific molecular- or cell-level endpoint. Furthermore, the ability of reagents used in human patients to reduce anxiety to affect morphogenesis in a way predicted by our computational model further supports a research program in which tools and concepts from cognitive science are used beyond brains, to address the complex navigation of cell collectives in their anatomical problem space[13].

Our study had a number of limitations, which can be overcome in future work. First, because we wanted to isolate and understand the evolutionary properties of one specific mechanism, we focused on bioelectricity; numerous other developmental mechanisms – including biomechanics, chemical gradients, etc. – could be included to determine whether and how these influence the evolutionary process. Also, in our simulations, the indirect pattern organisms didn’t show the emergent competency to be robust to changes to initial morphological conditions (see ‘Morphological robustness’ experiment). This is in contrast with many systems in biology, which show high adaptability to different initial conditions. The task of learning the indirect mapping is harder than learning a direct one, demonstrating here likely the limits of our learning algorithm, even if we found in some cases some outliers with organisms that could show an appropriate development but only to specific changes in initial conditions. Our system also had a static bioelectrical pattern, which is a simplification of highly dynamical bioelectrical patterns for development that will be implemented in future iterations of our model. Finally, we don’t have access to the exact regulatory logic of the neural network

inside the cells, indeed, neural network interpretation is a difficult and on-going challenge[184-188], and using NCAs, e.g. network of networks adds a layer of complexity, which we will undertake in future work as tools for network interpretation.

One purpose of this kind of simulation is investigating the computational role and encoding of bioelectrical patterns in morphogenesis, with the aim to uncover novel mechanisms of development and evolution. This knowledge is fundamental, not only for basic evolutionary developmental biology but also for biomedicine and synthetic bioengineering by allowing the development of a rational control over large-scale growth and form and potentially paving the way for innovative therapeutic strategies in regenerative medicine and bioengineering targeting anatomical setpoints[68,189,190].

### Acknowledgements

We thank Julia Poirier for assistance in the manuscript.

### Conflict of Interest Statement

Tufts University and the Levin lab have a sponsored research agreement with Morphoceuticals, a company that operates in the regenerative therapeutics space and hopes to use bioelectricity as a repair modality.

### References

1. Pezzulo, G.; Levin, M. Re-membering the body: applications of computational neuroscience to the top-down control of regeneration of limbs and other complex organs. *Integr Biol (Camb)* **2015**, *7*, 1487-1517, doi:10.1039/c5ib00221d.
2. McCusker, C.; Gardiner, D.M. The axolotl model for regeneration and aging research: a mini-review. *Gerontology* **2011**, *57*, 565-571, doi:10.1159/000323761.
3. Vieira, W.A.; Wells, K.M.; McCusker, C.D. Advancements to the Axolotl Model for Regeneration and Aging. *Gerontology* **2020**, *66*, 212-222, doi:10.1159/000504294.
4. Pinet, K.; McLaughlin, K.A. Mechanisms of physiological tissue remodeling in animals: Manipulating tissue, organ, and organism morphology. *Dev Biol* **2019**, *451*, 134-145, doi:10.1016/j.ydbio.2019.04.001.
5. Pinet, K.; Deolankar, M.; Leung, B.; McLaughlin, K.A. Adaptive correction of craniofacial defects in pre-metamorphic *Xenopus laevis* tadpoles involves thyroid hormone-independent tissue remodeling. *Development* **2019**, *146*, doi:10.1242/dev.175893.
6. Harris, A.K. The need for a concept of shape homeostasis. *Biosystems* **2018**, *173*, 65-72, doi:10.1016/j.biosystems.2018.09.012.
7. Andersen, T.; Newman, R.; Otter, T. Shape homeostasis in virtual embryos. *Artif Life* **2009**, *15*, 161-183, doi:10.1162/artl.2009.15.2.15201.
8. Stone, J.R. The spirit of D'Arcy Thompson dwells in empirical morphospace. *Math Biosci* **1997**, *142*, 13-30, doi:10.1016/s0025-5564(96)00186-1.

TMBMC-TPS-25-0025

9. Abzhanov, A.; Protas, M.; Grant, B.R.; Grant, P.R.; Tabin, C.J. Bmp4 and morphological variation of beaks in Darwin's finches. *Science* **2004**, *305*, 1462-1465, doi:10.1126/science.1098095.
10. Raup, D.M.; Michelson, A. Theoretical Morphology of the Coiled Shell. *Science* **1965**, *147*, 1294-1295, doi:10.1126/science.147.3663.1294.
11. Foote, M. The evolution of morphological diversity. *Annual Review of Ecology and Systematics* **1997**, *28*, 129-152, doi:10.1146/annurev.ecolsys.28.1.129.
12. Levin, M. Collective Intelligence of Morphogenesis as a Teleonomic Process. In *Evolution "on Purpose"*: *Teleonomy in Living Systems*, Corning, P.A., Kauffman, S. A., Noble, D., Shapiro, J. A., Vane-Wright, R. I., Pross, A., Ed.; MIT Press: Cambridge, 2023; pp. 175-198.
13. Fields, C.; Levin, M. Competency in Navigating Arbitrary Spaces as an Invariant for Analyzing Cognition in Diverse Embodiments. *Entropy-Switz* **2022**, *24*, 819, doi:10.3390/e24060819.
14. Levin, M. Bioelectric signaling: Reprogrammable circuits underlying embryogenesis, regeneration, and cancer. *Cell* **2021**, *184*, 1971-1989, doi:10.1016/j.cell.2021.02.034.
15. Munjal, A.; Philippe, J.M.; Munro, E.; Lecuit, T. A self-organized biomechanical network drives shape changes during tissue morphogenesis. *Nature* **2015**, *524*, 351-355, doi:10.1038/nature14603.
16. Robertson, M. Retinoic acid receptor. Towards a biochemistry of morphogenesis. *Nature* **1987**, *330*, 420-421, doi:10.1038/330420a0.
17. Kindberg, A.; Hu, J.K.; Bush, J.O. Forced to communicate: Integration of mechanical and biochemical signaling in morphogenesis. *Curr Opin Cell Biol* **2020**, *66*, 59-68, doi:10.1016/j.ceb.2020.05.004.
18. Shim, G.; Breinyn, I.B.; Martinez-Calvo, A.; Rao, S.; Cohen, D.J. Bioelectric stimulation controls tissue shape and size. *Nat Commun* **2024**, *15*, 2938, doi:10.1038/s41467-024-47079-w.
19. Harris, M.P. Bioelectric signaling as a unique regulator of development and regeneration. *Development* **2021**, *148*, dev180794, doi:10.1242/dev.180794.
20. George, L.F.; Bates, E.A. Mechanisms Underlying Influence of Bioelectricity in Development. *Front Cell Dev Biol* **2022**, *10*, 772230, doi:10.3389/fcell.2022.772230.
21. Bates, E. Ion Channels in Development and Cancer. *Annu Rev Cell Dev Biol* **2015**, *31*, 231-247, doi:10.1146/annurev-cellbio-100814-125338.
22. Schofield, Z.; Meloni, G.N.; Tran, P.; Zerfass, C.; Sena, G.; Hayashi, Y.; Grant, M.; Contera, S.A.; Minteer, S.D.; Kim, M.; et al. Bioelectrical understanding and engineering of cell biology. *J R Soc Interface* **2020**, *17*, 20200013, doi:10.1098/rsif.2020.0013.
23. Funk, R.H.W.; Scholkmann, F. The significance of bioelectricity on all levels of organization of an organism. Part 1: From the subcellular level to cells. *Prog Biophys Mol Biol* **2023**, *177*, 185-201, doi:10.1016/j.pbiomolbio.2022.12.002.
24. Funk, R. Ion Gradients in Tissue and Organ Biology. *Biological Systems* **2013**, doi:doi:10.4172/bso.1000105.
25. Adams, D.S.; Uzel, S.G.; Akagi, J.; Wlodkowic, D.; Andreeva, V.; Yelick, P.C.; Devitt-Lee, A.; Pare, J.F.; Levin, M. Bioelectric signalling via potassium channels: a mechanism for craniofacial dysmorphogenesis in KCNJ2-associated Andersen-Tawil Syndrome. *J Physiol* **2016**, *594*, 3245-3270, doi:10.1113/JPhysiol.2016.1930.
26. Vandenberg, L.N.; Morrie, R.D.; Adams, D.S. V-ATPase-dependent ectodermal voltage and pH regionalization are required for craniofacial morphogenesis. *Dev Dyn* **2011**, *240*, 1889-1904, doi:10.1002/dvdy.22685.
27. Emmons-Bell, M.; Durant, F.; Hammelman, J.; Bessonov, N.; Volpert, V.; Morokuma, J.; Pinet, K.; Adams, D.S.; Pietak, A.; Lobo, D.; et al. Gap Junctional Blockade Stochastically Induces Different Species-Specific Head Anatomies in Genetically Wild-Type Girardia dorotocephala Flatworms. *Int J Mol Sci* **2015**, *16*, 27865-27896, doi:10.3390/ijms161126065.
28. Stern, C.D. Experimental reversal of polarity in chick embryo epiblast sheets in vitro. *Exp Cell Res* **1982**, *140*, 468-471, doi:10.1016/0014-4827(82)90143-4.
29. Beane, W.S.; Morokuma, J.; Adams, D.S.; Levin, M. A Chemical genetics approach reveals H,K-ATPase-mediated membrane voltage is required for planarian head regeneration. *Chemistry & Biology* **2011**, *18*, 77-89, doi:10.1016/j.chembiol.2010.11.012.
30. Durant, F.; Bischoff, J.; Fields, C.; Morokuma, J.; LaPalme, J.; Hoi, A.; Levin, M. The Role of Early Bioelectric Signals in the Regeneration of Planarian Anterior/Posterior Polarity. *Biophys J* **2019**, *116*, 948-961, doi:10.1016/j.bpj.2019.01.029.
31. Levin, M.; Thorlin, T.; Robinson, K.R.; Nogi, T.; Mercola, M. Asymmetries in H<sup>+</sup>/K<sup>+</sup>-ATPase and cell membrane potentials comprise a very early step in left-right patterning. *Cell* **2002**, *111*, 77-89, doi:10.1016/s0092-8674(02)00939-x.
32. Adams, D.S.; Robinson, K.R.; Fukumoto, T.; Yuan, S.; Albertson, R.C.; Yelick, P.; Kuo, L.; McSweeney, M.; Levin, M. Early, H<sup>+</sup>-V-ATPase-dependent proton flux is necessary for consistent left-right patterning of non-mammalian vertebrates. *Development* **2006**, *133*, 1657-1671, doi:10.1242/dev.02341.
33. Pai, V.P.; Aw, S.; Shomrat, T.; Lemire, J.M.; Levin, M. Transmembrane voltage potential controls embryonic eye patterning in *Xenopus laevis*. *Development* **2012**, *139*, 313-323, doi:10.1242/dev.073759.
34. Nuckles, R.J.; Ng, A.; Darland, T.; Gross, J.M. The vacuolar-ATPase complex regulates retinoblast proliferation and survival, photoreceptor morphogenesis, and pigmentation in the zebrafish eye. *Investigative ophthalmology & visual science* **2009**, *50*, 893-905, doi:10.1167/iovs.08-2743.
35. Emmons-Bell, M.; Hariharan, I.K. Membrane potential regulates Hedgehog signalling in the *Drosophila* wing imaginal disc. *EMBO Rep* **2021**, *22*, e51861, doi:10.15252/embr.202051861.
36. George, L.F.; Pradhan, S.J.; Mitchell, D.; Josey, M.; Casey, J.; Belus, M.T.; Dahal, G.R.; Bates, E.A. Ion Channel Contributions to Wing Development in *Drosophila melanogaster*. *G3 (Bethesda)* **2019**, *9*, 999-1008, doi:10.1534/g3.119.400028.
37. Dahal, G.R.; Pradhan, S.J.; Bates, E.A. Inwardly rectifying potassium channels influence *Drosophila* wing morphogenesis by regulating Dpp release. *Development* **2017**, *144*, 2771-2783, doi:10.1242/dev.146647.
38. Dahal, G.R.; Rawson, J.; Gassaway, B.; Kwok, B.; Tong, Y.; Ptacek, L.J.; Bates, E. An inwardly rectifying K<sup>+</sup> channel is required for patterning. *Development* **2012**, *139*, 3653-3664, doi:10.1242/dev.078592.
39. Schotthofer, S.K.; Bohrmann, J. Analysing bioelectrical phenomena in the *Drosophila* ovary with genetic tools: tissue-specific expression of sensors for membrane potential and intracellular pH, and RNAi-knockdown of mechanisms involved in ion exchange. *BMC Dev Biol* **2020**, *20*, 15, doi:10.1186/s12861-020-00220-6.

TMBMC-TPS-25-0025

40. Weiss, I.; Bohrmann, J. Electrochemical gradients are involved in regulating cytoskeletal patterns during epithelial morphogenesis in the *Drosophila* ovary. *BMC Dev Biol* **2019**, *19*, 22, doi:10.1186/s12861-019-0203-y.
41. Weiss, I.; Bohrmann, J. Electrochemical patterns during *Drosophila* oogenesis: ion-transport mechanisms generate stage-specific gradients of pH and membrane potential in the follicle-cell epithelium. *Bmc Developmental Biology* **2019**, *19*, 12, doi:10.1186/s12861-019-0192-x.
42. Woodruff, R.I.; Telfer, W.H. Polarized intercellular bridges in ovarian follicles of the cecropia moth. *J Cell Biol* **1973**, *58*, 172-188, doi:10.1083/jcb.58.1.172.
43. Telfer, W.H.; Woodruff, R.I. Ion physiology of vitellogenetic follicles. *J Insect Physiol* **2002**, *48*, 915-923, doi:10.1016/s0022-1910(02)00152-x.
44. Jiang, T.-X.; Li, A.; Lin, C.-M.; Chiu, C.; Cho, J.-H.; Reid, B.; Zhao, M.; Chow, R.H.; Widelitz, R.B.; Chuong, C.-M. Global feather orientations changed by electric current. *iScience* **2021**, *24*, 102671, doi:<https://doi.org/10.1016/j.isci.2021.102671>.
45. Silic, M.R.; Zhang, G. Bioelectricity in Developmental Patterning and Size Control: Evidence and Genetically Encoded Tools in the Zebrafish Model. *Cells* **2023**, *12*, doi:10.3390/cells12081148.
46. Yi, C.; Spitters, T.W.; Al-Far, E.A.A.; Wang, S.; Xiong, T.; Cai, S.; Yan, X.; Guan, K.; Wagner, M.; El-Armouche, A.; et al. A calcineurin-mediated scaling mechanism that controls a K<sup>(+)</sup>-leak channel to regulate morphogen and growth factor transcription. *Elife* **2021**, *10*, doi:10.7554/elife.60691.
47. Kujawski, S.; Lin, W.; Kitte, F.; Bormel, M.; Fuchs, S.; Arulmozhivarman, G.; Vogt, S.; Theil, D.; Zhang, Y.; Antos, C.L. Calcineurin regulates coordinated outgrowth of zebrafish regenerating fins. *Developmental cell* **2014**, *28*, 573-587, doi:10.1016/j.devcel.2014.01.019.
48. Perathoner, S.; Daane, J.M.; Henrion, U.; Seeböhm, G.; Higdon, C.W.; Johnson, S.L.; Nusslein-Volhard, C.; Harris, M.P. Bioelectric signaling regulates size in zebrafish fins. *PLoS Genet* **2014**, *10*, e1004080, doi:10.1371/journal.pgen.1004080.
49. Belus, M.T.; Rogers, M.A.; Elzubeir, A.; Josey, M.; Rose, S.; Andreeva, V.; Yelick, P.C.; Bates, E.A. Kir2.1 is important for efficient BMP signaling in mammalian face development. *Dev Biol* **2018**, *444 Suppl 1*, S297-S307, doi:10.1016/j.ydbio.2018.02.012.
50. Pai, V.P.; Martyniuk, C.J.; Echeverri, K.; Sundelacruz, S.; Kaplan, D.L.; Levin, M. Genome-wide analysis reveals conserved transcriptional responses downstream of resting potential change in *Xenopus* embryos, axolotl regeneration, and human mesenchymal cell differentiation. *Regeneration (Oxf)* **2016**, *3*, 3-25, doi:10.1002/regb.248.
51. Chernet, B.T.; Levin, M. Transmembrane voltage potential is an essential cellular parameter for the detection and control of tumor development in a *Xenopus* model. *Dis Model Mech* **2013**, *6*, 595-607, doi:10.1242/dmm.010835.
52. Sundelacruz, S.; Levin, M.; Kaplan, D.L. Role of membrane potential in the regulation of cell proliferation and differentiation. *Stem cell reviews and reports* **2009**, *5*, 231-246, doi:10.1007/s12015-009-9080-2.
53. Blackiston, D.J.; McLaughlin, K.A.; Levin, M. Bioelectric controls of cell proliferation: ion channels, membrane voltage and the cell cycle. *Cell cycle (Georgetown, Tex)* **2009**, *8*, 3519-3528, doi:10.4161/cc.8.21.9888.
54. Carvalho, J. A computational model of cell membrane bioelectric polarization and depolarization, connected with cell proliferation, in different tissue geometries. *J Theor Biol* **2023**, *557*, 111338, doi:10.1016/j.jtbi.2022.111338.
55. Pietak, A.; Levin, M. Bioelectrical control of positional information in development and regeneration: A review of conceptual and computational advances. *Prog Biophys Mol Biol* **2018**, *137*, 52-68, doi:10.1016/j.pbiomolbio.2018.03.008.
56. Pietak, A.; Levin, M. Bioelectric gene and reaction networks: computational modelling of genetic, biochemical and bioelectrical dynamics in pattern regulation. *J R Soc Interface* **2017**, *14*, doi:10.1098/rsif.2017.0425.
57. Cervera, J.; Levin, M.; Mafe, S. Morphology changes induced by intercellular gap junction blocking: A reaction-diffusion mechanism. *Biosystems* **2021**, *209*, 104511, doi:10.1016/j.biosystems.2021.104511.
58. Cervera, J.; Meseguer, S.; Levin, M.; Mafe, S. Bioelectrical model of head-tail patterning based on cell ion channels and intercellular gap junctions. *Bioelectrochemistry* **2020**, *132*, 107410, doi:10.1016/j.bioelechem.2019.107410.
59. Lobo, D.; Beane, W.S.; Levin, M. Modeling planarian regeneration: a primer for reverse-engineering the worm. *PLoS Comput Biol* **2012**, *8*, e1002481, doi:10.1371/journal.pcbi.1002481.
60. Sheiman, I.M.; Kreshchenko, N.D. Regeneration of Planarians: Experimental Object. *Russ J Dev Biol+* **2015**, *46*, 1-9, doi:Doi 10.1134/S1062360415010075.
61. Cebrià, F.; Adell, T.; Saló, E. Rebuilding a planarian: from early signaling to final shape. *Int J Dev Biol* **2018**, *62*, 537-550, doi:10.1387/ijdb.180042es.
62. Oviedo, N.J.; Newmark, P.A.; Sanchez Alvarado, A. Allometric scaling and proportion regulation in the freshwater planarian *Schmidtea mediterranea*. *Dev Dyn* **2003**, *226*, 326-333, doi:10.1002/dvdy.10228.
63. Durant, F.; Morokuma, J.; Fields, C.; Williams, K.; Adams, D.S.; Levin, M. Long-Term, Stochastic Editing of Regenerative Anatomy via Targeting Endogenous Bioelectric Gradients. *Biophysical Journal* **2017**, *112*, 2231-2243, doi:10.1016/j.bpj.2017.04.011.
64. Pezzullo, G.; LaPalme, J.; Durant, F.; Levin, M. Bistability of somatic pattern memories: stochastic outcomes in bioelectric circuits underlying regeneration. *Philos Trans R Soc Lond B Biol Sci* **2021**, *376*, 20190765, doi:10.1098/rstb.2019.0765.
65. Oviedo, N.J.; Morokuma, J.; Walentek, P.; Kema, I.P.; Gu, M.B.; Ahn, J.M.; Hwang, J.S.; Gojobori, T.; Levin, M. Long-range neural and gap junction protein-mediated cues control polarity during planarian regeneration. *Dev Biol* **2010**, *339*, 188-199, doi:S0012-1606(09)01402-X [pii] 10.1016/j.ydbio.2009.12.012.
66. Beane, W.S.; Morokuma, J.; Lemire, J.M.; Levin, M. Bioelectric signaling regulates head and organ size during planarian regeneration. *Development* **2013**, *140*, 313-322, doi:10.1242/dev.086900.
67. Sullivan, K.G.; Emmons-Bell, M.; Levin, M. Physiological inputs regulate species-specific anatomy during embryogenesis and regeneration. *Commun Integr Biol* **2016**, *9*, e1192733, doi:10.1080/19420889.2016.1192733.
68. Pio-Lopez, L.; Levin, M. Morphaceuticals: Perspectives for discovery of drugs targeting anatomical control mechanisms in regenerative medicine, cancer and aging. *Drug Discov Today* **2023**, *28*, 103585, doi:10.1016/j.drudis.2023.103585.
69. Pio-Lopez, L.; Levin, M. Aging as a loss of morphostatic information: A developmental

- bioelectricity perspective. *Ageing Res Rev* **2024**, *97*, 102310, doi:10.1016/j.arr.2024.102310.
70. Levin, M.; Martyniuk, C.J. The bioelectric code: An ancient computational medium for dynamic control of growth and form. *Biosystems* **2018**, *164*, 76–93, doi:10.1016/j.biosystems.2017.08.009.
71. Bates, E.A. A potential molecular target for morphological defects of fetal alcohol syndrome: Kir2.1. *Curr Opin Genet Dev* **2013**, *23*, 324–329, doi:10.1016/j.gde.2013.05.001.
72. Lanni, J.S.; Peal, D.; Ekstrom, L.; Chen, H.; Stanclift, C.; Bowen, M.E.; Mercado, A.; Gamba, G.; Kahle, K.T.; Harris, M.P. Integrated K<sup>+</sup> channel and K+Cl<sup>-</sup> cotransporter functions are required for the coordination of size and proportion during development. *Dev Biol* **2019**, *456*, 164–178, doi:10.1016/j.ydbio.2019.08.016.
73. Parsons, K.J.; Son, Y.H.; Crespel, A.; Thambithurai, D.; Killen, S.; Harris, M.P.; Albertson, R.C. Conserved but flexible modularity in the zebrafish skull: implications for craniofacial evolvability. *Proc Biol Sci* **2018**, *285*, doi:10.1098/rspb.2017.2671.
74. Daane, J.M.; Lanni, J.; Rothenberg, I.; Seehoem, G.; Higdon, C.W.; Johnson, S.L.; Harris, M.P. Bioelectric-calcineurin signaling module regulates allometric growth and size of the zebrafish fin. *Sci Rep* **2018**, *8*, 10391, doi:10.1038/s41598-018-28450-6.
75. Petsakou, A.; Perrimon, N. Bioelectric regulation of intestinal stem cells. *Trends Cell Biol* **2023**, *33*, 555–567, doi:10.1016/j.tcb.2022.10.003.
76. Sundelacruz, S.; Moody, A.T.; Levin, M.; Kaplan, D.L. Membrane Potential Depolarization Alters Calcium Flux and Phosphate Signaling During Osteogenic Differentiation of Human Mesenchymal Stem Cells. *Bioelectricity* **2019**, *1*, 56–66, doi:10.1089/bioe.2018.0005.
77. Bautista, W.; Perez-Alvarez, V.; Burczynski, F.; Raouf, A.; Klonisch, T.; Minuk, G. Membrane potential differences and GABA<sub>A</sub> receptor expression in hepatic tumor and non-tumor stem cells. *Can J Physiol Pharmacol* **2014**, *92*, 85–91, doi:10.1139/cjpp-2013-0226.
78. Sun, Y.; Dong, Z.; Jin, T.; Ang, K.H.; Huang, M.; Haston, K.M.; Peng, J.; Zhong, T.P.; Finkbeiner, S.; Weiss, W.A.; et al. Imaging-based chemical screening reveals activity-dependent neural differentiation of pluripotent stem cells. *eLife* **2013**, *2*, e00508, doi:10.7554/eLife.00508.
79. Balasubramanian, S.; Weston, D.A.; Levin, M.; Davidian, D.C.C. Electroceuticals: emerging applications beyond the nervous system and excitable tissues. *Trends Pharmacol Sci* **2024**, *45*, 391–394, doi:10.1016/j.tips.2024.03.001.
80. Mathews, J.; Levin, M. The body electric 2.0: recent advances in developmental bioelectricity for regenerative and synthetic bioengineering. *Curr Opin Biotechnol* **2018**, *52*, 134–144, doi:10.1016/j.copbio.2018.03.008.
81. Davidian, D.; Levin, M. Inducing Vertebrate Limb Regeneration: A Review of Past Advances and Future Outlook. *Cold Spring Harb Perspect Biol* **2022**, *14*, doi:10.1101/csphperspect.a040782.
82. Barbieri, M. Biology with information and meaning. *Hist Philos Life Sci* **2003**, *25*, 243–254, doi:10.1080/03919710312331273045.
83. Barbieri, M. The organic codes. The basic mechanism of macroevolution. *Riv Biol* **1998**, *91*, 481–513.
84. Barbieri, M. A general model on the origin of biological codes. *Biosystems* **2019**, *181*, 11–19, doi:10.1016/j.biosystems.2019.04.010.
85. Barbieri, M. What is code biology? *Biosystems* **2018**, *164*, 1–10, doi:10.1016/j.biosystems.2017.10.005.
86. Lobo, D.; Solano, M.; Bubenik, G.A.; Levin, M. A linear-encoding model explains the variability of the target morphology in regeneration. *Journal of the Royal Society, Interface / the Royal Society* **2014**, *11*, 20130918, doi:10.1098/rsif.2013.0918.
87. Adams, D.S.; Masi, A.; Levin, M. H<sup>+</sup> pump-dependent changes in membrane voltage are an early mechanism necessary and sufficient to induce *Xenopus* tail regeneration. *Development* **2007**, *134*, 1323–1335, doi:10.1242/dev.02812.
88. Tseng, A.S.; Beane, W.S.; Lemire, J.M.; Masi, A.; Levin, M. Induction of vertebrate regeneration by a transient sodium current. *J Neurosci* **2010**, *30*, 13192–13200, doi:30/39/13192 [pii] 10.1523/JNEUROSCI.3315-10.2010.
89. Tseng, A.; Levin, M. Cracking the bioelectric code: Probing endogenous ionic controls of pattern formation. *Commun Integr Biol* **2013**, *6*, e22595, doi:10.4161/cib.22595.
90. Cervera, J.; Meseguer, S.; Mafe, S. Intercellular Connectivity and Multicellular Bioelectric Oscillations in Nonexcitable Cells: A Biophysical Model. *ACS Omega* **2018**, *3*, 13567–13575, doi:10.1021/acsomega.8b01514.
91. Cervera, J.; Manzanares, J.A.; Mafe, S. Cell-cell bioelectrical interactions and local heterogeneities in genetic networks: a model for the stabilization of single-cell states and multicellular oscillations. *Phys Chem Chem Phys* **2018**, *20*, 9343–9354, doi:10.1039/C8CP00648B.
92. Mordvintsev, A.; Randazzo, E.; Niklasson, E.; Levin, M. Growing Neural Cellular Automata. *Distill* **2020**, *5*, e23, doi:10.23915/distill.00023.
93. Horibe, K.; Walker, K.; Risi, S. Regenerating soft robots through neural cellular automata. In *Genetic Programming, EuroGP 2021*, Hu, T., Lourenço, N., Medvet, E., Eds.; Lecture Notes in Computer Science; Springer: Cham, 2021; pp. 36–50.
94. Najarro, E.; Sudhakaran, S.; Glanois, C.; Risi, S. Hypernca: Growing developmental networks with neural cellular automata. *arXiv preprint arXiv:2204.11674* **2022**, doi:10.48550/arXiv.2204.11674.
95. Stovold, J. Neural cellular automata can respond to signals. In Proceedings of the ALIFE 2023: Ghost in the Machine, 2023.
96. Shreesha, L.; Levin, M. Stress sharing as cognitive glue for collective intelligences: A computational model of stress as a coordinator for morphogenesis. *Biochem Biophys Res Commun* **2024**, *731*, 150396, doi:10.1016/j.bbrc.2024.150396.
97. Pio-Lopez, L.; Bischof, J.; LaPalme, J.V.; Levin, M. The scaling of goals from cellular to anatomical homeostasis: an evolutionary simulation, experiment and analysis. *Interface Focus* **2023**, *13*, 20220072, doi:10.1098/rsfs.2022.0072.
98. Sharpe, J. Wolpert's French Flag: what's the problem? *Development* **2019**, *146*, doi:10.1242/dev.185967.
99. Wolpert, L. Positional information and the spatial pattern of cellular differentiation. *J Theor Biol* **1969**, *25*, 1–47, doi:10.1016/s0022-5193(69)80016-0.
100. Wolpert, L. The French Flag Problems A Contribution to the Discussion on Pattern Development and Regulation. In *The Origin of Life*, Waddington, C.H., Ed.; Routledge: 2017; pp. 125–133.
101. Vadde, B.V.L.; Roeder, A.H.K. Can the French flag and reaction-diffusion models explain flower patterning? Celebrating the 50th anniversary of the

- French flag model. *J Exp Bot* **2020**, *71*, 2886-2897, doi:10.1093/jxb/era065.
102. Bowers, C.P. Formation of modules in a computational model of embryogeny. *Ieee C Evol Computat* **2005**, *1*, 537-542, doi:10.1109/CEC.2005.1554729.
103. Hillenbrand, P.; Gerland, U.; Tkačik, G. Beyond the French Flag Model: Exploiting Spatial and Gene Regulatory Interactions for Positional Information. *PLoS One* **2016**, *11*, e0163628, doi:10.1371/journal.pone.0163628.
104. Ancona, B.; Bajwa, A.; Lynch, N.; Mallmann-Trenn, F. How to Color a French Flag. In *Structural Information and Communication Complexity*; Censor-Hillel, K., Flammini, M., Eds.; Lecture Notes in Computer Science; Springer: Cham, 2019; pp. 327-331.
105. Kremer, S.; Vercelli, G.; Gerland, U. The French Flag Problem Revisited: Creating Robust and Tunable Axial Patterns Without Global Signaling. *eLife* **2024**, *13*, RP94699, doi:10.7554/eLife.94699.1.
106. Chavoya, A.; Duthen, Y. Using a genetic algorithm to evolve cellular automata for 2D/3D computational development. In Proceedings of the GECCO '06: 8th annual conference on Genetic and evolutionary computation, Seattle, WA, 2006; pp. 231 - 232.
107. Chavoya, A.; Duthen, Y. Use of a genetic algorithm to evolve an extended artificial regulatory network for cell pattern generation. In Proceedings of the GECCO '07: 9th annual conference on Genetic and evolutionary computation, London, UK, 2007; p. 1062.
108. Lee, H.C.; Hastings, C.; Oliveira, N.M.M.; Pérez-Carrasco, R.; Page, K.M.; Wolpert, L.; Stern, C.D. 'Neighbourhood watch' model: embryonic epiblast cells assess positional information in relation to their neighbours. *Development* **2022**, *149*, dev200295, doi:10.1242/dev.200295.
109. Grasso, C.; Bongard, J. Empowered Neural Cellular Automata. In Proceedings of the GECCO '22: Genetic and Evolutionary Computation Conference, Boston, MA, 2022; pp. 108-111.
110. Hartl, B.; Risi, S.; Levin, M. Evolutionary Implications of Self-Assembling Cybernetic Materials with Collective Problem-Solving Intelligence at Multiple Scales. *Entropy (Basel)* **2024**, *26*, 532, doi:10.3390/e26070532.
111. Ravelo, M.A. Artificial morphogenesis via 3D neural cellular automata. The University of Texas at Austin, 2024.
112. Mordvintsev, A.; Randazzo, E.; Fouts, C. Growing isotropic neural cellular automata. In Proceedings of the The 2022 Conference on Artificial Life, Trento, Italy, 2022, 2022; p. 65.
113. Ruiz, A.H.; Vilalta, A.; Moreno-Noguer, F. Neural cellular automata manifold. In Proceedings of the IEEE/CVF Conference on Computer Vision and Pattern Recognition (CVPR), Nashville, TN, 2021; pp. 10015-10023.
114. Sudhakaran, S.; Grbic, D.; Li, S.; Katona, A.; Najarro, E.; Glanois, C.; Risi, S., . Growing 3d artefacts and functional machines with neural cellular automata. In Proceedings of the ALIFE 2021: The 2021 Conference on Artificial Life 2021.
115. Pande, R.; Grattarola, D. Heirarchical neural cellular automata. In Proceedings of the ALIFE 2023: Ghost in the Machine, 2023.
116. Manicka, S.; Pai, V.P.; Levin, M. Information integration during bioelectric regulation of morphogenesis of the embryonic frog brain. *iScience* **2023**, *26*, 108398, doi:10.1016/j.isci.2023.108398.
117. Vandenberg, L.N.; Adams, D.S.; Levin, M. Normalized shape and location of perturbed craniofacial structures in the Xenopus tadpole reveal an innate ability to achieve correct morphology. *Dev Dyn* **2012**, *241*, 863-878, doi:10.1002/dvdy.23770.
118. Vohradsky, J. Neural model of the genetic network. *J Biol Chem* **2001**, *276*, 36168-36173, doi:10.1074/jbc.M104391200.
119. Sorek, M.; Balaban, N.Q.; Loewenstein, Y. Stochasticity, bistability and the wisdom of crowds: a model for associative learning in genetic regulatory networks. *PLoS Comput Biol* **2013**, *9*, e1003179, doi:10.1371/journal.pcbi.1003179.
120. Watson, R.; Buckley, C.L.; Mills, R.; Davies, A. Associative memory in gene regulation networks. In Proceedings of the ALIFE 2012: 12th International Conference on the Synthesis and Simulation of Living Systems Odense, Denmark, 2010; pp. 194-202.
121. Watson, R.A.; Wagner, G.P.; Pavlicev, M.; Weinreich, D.M.; Mills, R. The evolution of phenotypic correlations and "developmental memory". *Evolution* **2014**, *68*, 1124-1138, doi:10.1111/evol.12337.
122. Szabó, Á.; Vattay, G.; Kondor, D. A cell signaling model as a trainable neural nanonetwork. *Nano Communication Networks* **2012**, *3*, 57-64, doi:10.1016/j.nancom.2012.01.002.
123. Vey, G. Gene Coexpression as Hebbian Learning in Prokaryotic Genomes. *B Math Biol* **2013**, *75*, 2431-2449, doi:10.1007/s11538-013-9900-z.
124. Herrera-Delgado, E.; Perez-Carrasco, R.; Briscoe, J.; Sollich, P. Memory functions reveal structural properties of gene regulatory networks. *PLoS Comput Biol* **2018**, *14*, e1006003, doi:10.1371/journal.pcbi.1006003.
125. Csermely, P.; Kunscí, N.; Mendik, P.; Kerestély, M.; Faragó, T.; Veres, D.V.; Tompa, P. Learning of Signaling Networks: Molecular Mechanisms. *Trends Biochem Sci* **2020**, *45*, 284-294, doi:10.1016/j.tibs.2019.12.005.
126. Niraula, D.; El Naqa, I.; Tuszyński, J.A.; Gatenby, R.A. Modeling non-genetic information dynamics in cells using reservoir computing. *iScience* **2024**, *27*, 109614, doi:10.1016/j.isci.2024.109614.
127. Risi, S.; Stanley, K.O. An enhanced hypercube-based encoding for evolving the placement, density, and connectivity of neurons. *Artif Life* **2012**, *18*, 331-363, doi:10.1162/ARTL\_a\_00071.
128. Risi, S.; Lehman, J.; Stanley, K.O. Evolving the placement and density of neurons in the hyperneat substrate. In Proceedings of the GECCO '10: 12th annual conference on Genetic and evolutionary computation, Portland, Oregon, 2010; pp. 563-570.
129. Risi, S.; Stanley, K.O. Enhancing es-hyperneat to evolve more complex regular neural networks. In Proceedings of the GECCO '11: 13th annual conference on Genetic and evolutionary computation, Dublin, Ireland, 2011, 2011; pp. 1539-1546.
130. D'Ambrosio, D.B.; Gauci, J.; Stanley, K.O. HyperNEAT: The First Five Years. In *Growing Adaptive Machines*; Kowaliw, T., Bredeche, N., Doursat, R., Eds.; Studies in Computational Intelligence; Springer: Berlin, Heidelberg, 2014; pp. 159-185.
131. Stanley, K.O.; D'Ambrosio, D.B.; Gauci, J. A hypercube-based encoding for evolving large-scale neural networks. *Artif Life* **2009**, *15*, 185-212, doi:10.1162/artl.2009.15.2.15202.
132. Kazil, J.; Masad, D.; Crooks, A. Utilizing Python for Agent-Based Modeling: The Mesa Framework. In *Social, Cultural, and Behavioral Modeling*, Thomson, R., Bisgin, H., Dancy, C., Hyder, A., Hussain, M., Eds.;

TMBMC-TPS-25-0025

- Lecture Notes in Computer Science; Springer: Cham, 2020; pp. 308-317.
133. Masad, D.; Kazil, J.L. Mesa: An Agent-Based Modeling Framework. In Proceedings of the 14th annual Scientific Computing with Python conference, Austin, TX, 2015; pp. 51-58.
134. Oviedo, N.J.; Nicolas, C.L.; Adams, D.S.; Levin, M. Establishing and maintaining a colony of planarians. *CSH Protoc* **2008**, *2008*, pdb prot5053, doi:10.1101/pdb.prot5053.
135. Keller, E.F. Developmental robustness. *Ann N Y Acad Sci* **2002**, *981*, 189-201, doi:10.1111/j.1749-6632.2002.tb04918.x.
136. Mestek Boukhbar, L.; Barkoulas, M. The developmental genetics of biological robustness. *Ann Bot* **2016**, *117*, 699-707, doi:10.1093/aob/mcv128.
137. Gursky, V.V.; Surkova, S.Y.; Samsonova, M.G. Mechanisms of developmental robustness. *Biosystems* **2012**, *109*, 329-335, doi:10.1016/j.biosystems.2012.05.013.
138. Blackiston, D.J.; Levin, M. Ectopic eyes outside the head in Xenopus tadpoles provide sensory data for light-mediated learning. *J Exp Biol* **2013**, *216*, 1031-1040, doi:10.1242/jeb.074963.
139. Yakushiji, N.; Yokoyama, H.; Tamura, K. Repatterning in amphibian limb regeneration: A model for study of genetic and epigenetic control of organ regeneration. *Semin Cell Dev Biol* **2009**, *20*, 565-574, doi:10.1016/j.semcd.2008.12.007.
140. Wake, D.B.; Hanken, J. Direct development in the lungless salamanders: what are the consequences for developmental biology, evolution and phylogenesis? *Int J Dev Biol* **1996**, *40*, 859-869.
141. Worley, M.I.; Hariharan, I.K. Imaginal Disc Regeneration: Something Old, Something New. *Cold Spring Harb Perspect Biol* **2022**, *14*, doi:10.1101/cshperspect.a040733.
142. Healy, D.; LaPalme, J.; Levin, M. Post-SSRI Sexual Dysfunction: A Bioelectric Mechanism? *Bioelectricity* **2020**, *2*, 7-13, doi:10.1089/bioe.2019.0010.
143. DeLucia, V.; Kelsberg, G.; Safranek, S. Which SSRIs most effectively treat depression in adolescents? *J Fam Pract* **2016**, *65*, 632-634.
144. Ferguson, J.M. SSRI Antidepressant Medications: Adverse Effects and Tolerability. *Prim Care Companion J Clin Psychiatry* **2001**, *3*, 22-27, doi:10.4088/pcc.v03n0105.
145. Papakostas, G.I.; Fava, M.; Thase, M.E. Treatment of SSRI-resistant depression: a meta-analysis comparing within- versus across-class switches. *Biol Psychiatry* **2008**, *63*, 699-704, doi:10.1016/j.biopsych.2007.08.010.
146. Blattner, M.; Levin, M. Long Range Communication via Gap Junctions and Stress in Planarian Morphogenesis: A Computational Study. *Bioelectricity* **2023**, *5*, 196-209, doi:10.1089/bioe.2023.0032.
147. Hernández-Díaz, S.; Levin, M. Alteration of bioelectrically-controlled processes in the embryo: a teratogenic mechanism for anticonvulsants. *Reprod Toxicol* **2014**, *47*, 111-114, doi:10.1016/j.reprotox.2014.04.008.
148. Fischer, A.G.; Ullsperger, M. An Update on the Role of Serotonin and its Interplay with Dopamine for Reward. *Front Hum Neurosci* **2017**, *11*, 484, doi:10.3389/fnhum.2017.00484.
149. Kranz, G.S.; Kasper, S.; Lanzenberger, R. Reward and the serotonergic system. *Neuroscience* **2010**, *166*, 1023-1035, doi:10.1016/j.neuroscience.2010.01.036.
150. Nakatani, Y.; Amano, T. Functional Modulation of Na(v)1.2 Voltage-Gated Sodium Channels Induced by Escitalopram. *Biol Pharm Bull* **2018**, *41*, 1471-1474, doi:10.1248/bpb.b18-00214.
151. Hong, D.H.; Li, H.; Kim, H.S.; Shin, S.E.; Jung, W.K.; Na, S.H.; Choi, I.W.; Firth, A.L.; Park, W.S.; et al. The Effects of the Selective Serotonin Reuptake Inhibitor Fluvoxamine on Voltage-Dependent K(+) Channels in Rabbit Coronary Arterial Smooth Muscle Cells. *Biol Pharm Bull* **2015**, *38*, 1208-1213, doi:10.1248/bpb.b15-00207.
152. Albert, R.; Robeva, R.S. Signaling Networks: Asynchronous Boolean Models. In *Algebraic and Discrete Mathematical Methods for Modern Biology*, Robeva, R.S., Ed.; Academic Press: Boston, 2015; pp. 65-91.
153. Lobikin, M.; Chernet, B.; Lobo, D.; Levin, M. Resting potential, oncogene-induced tumorigenesis, and metastasis: the bioelectric basis of cancer *in vivo*. *Phys Biol* **2012**, *9*, 065002, doi:10.1088/1478-3975/9/6/065002.
154. Singer, M.L.; Oreschak, K.; Rhinehart, Z.; Robison, B.D. Anxiolytic effects of fluoxetine and nicotine exposure on exploratory behavior in zebrafish. *PeerJ* **2016**, *4*, e2352, doi:10.7717/peerj.2352.
155. Marcon, M.; Herrmann, A.P.; Mocelin, R.; Rambo, C.L.; Koakoski, G.; Abreu, M.S.; Conterato, G.M.; Kist, L.W.; Bogo, M.R.; Zanatta, L.; et al. Prevention of unpredictable chronic stress-related phenomena in zebrafish exposed to bromazepam, fluoxetine and nortriptyline. *Psychopharmacology (Berl)* **2016**, *233*, 3815-3824, doi:10.1007/s00213-016-4408-5.
156. Giacomini, A.C.V.; Abreu, M.S.; Giacomini, L.V.; Siebel, A.M.; Zimerman, F.F.; Rambo, C.L.; Mocelin, R.; Bonan, C.D.; Piatto, A.L.; Barcellos, L.J.G. Fluoxetine and diazepam acutely modulate stress induced-behavior. *Behav Brain Res* **2016**, *296*, 301-310, doi:10.1016/j.bbr.2015.09.027.
157. Al Shuraiqi, A.; Abed, R.M.M.; Al-Habsi, A.; Barry, M.J. Personality Affects Zebrafish Response to Sertraline. *Environ Toxicol Chem* **2024**, *43*, 132-146, doi:10.1002/etc.5769.
158. Mahase, E. Sertraline is better at reducing anxiety than depressive symptoms. *Bmj-Brit Med J* **2019**, *366*, i5655, doi:10.1136/bmj.i5655.
159. Hirschfeld, R.M. Sertraline in the treatment of anxiety disorders. *Depress Anxiety* **2000**, *11*, 139-157, doi:10.1002/1520-6394(2000)11:4<139::AID-DAI>3.0.CO;2-C.
160. Manassis, K.; Bradley, S. Fluoxetine in anxiety disorders. *J Am Acad Child Adolesc Psychiatry* **1994**, *33*, 761-762, doi:10.1097/00004583-199406000-00025.
161. Ofoegbu, P.U.; Campos, D.; Soares, A.; Pestana, J.L.T. Combined effects of NaCl and fluoxetine on the freshwater planarian, Schmidtea mediterranea (Platyhelminthes: Dugesiidae). *Environ Sci Pollut Res Int* **2019**, *26*, 11326-11335, doi:10.1007/s11356-019-04532-4.
162. Ofoegbu, P.U.; Lourenco, J.; Mendo, S.; Soares, A.; Pestana, J.L.T. Effects of low concentrations of psychiatric drugs (carbamazepine and fluoxetine) on the freshwater planarian, Schmidtea mediterranea. *Chemosphere* **2019**, *217*, 542-549, doi:10.1016/j.chemosphere.2018.10.198.
163. Chan, J.D.; Agbedanu, P.N.; Zamanian, M.; Gruba, S.M.; Haynes, C.L.; Day, T.A.; Marchant, J.S. 'Death and axes': unexpected Ca(2)(+) entry phenologs predict new anti-schistosomal agents. *PLoS Pathog* **2014**, *10*, e1003942, doi:10.1371/journal.ppat.1003942.
164. Montgomery, S.A.; McIntyre, A.; Osterheider, M.; Sarteschi, P.; Zitterl, W.; Zohar, J.; Birkett, M.; Wood, A.J. A double-blind, placebo-controlled study of

- fluoxetine in patients with DSM-III-R obsessive-compulsive disorder. The Lilly European OCD Study Group. *Eur Neuropsychopharmacol* **1993**, *3*, 143–152, doi:10.1016/0924-977x(93)90266-o.
165. Puscas, A.; Winiarski, M.; Leski, S.; Charzewski, L.; Nikolaei, T.; Borowska, J.; Dzik, J.M.; Bijata, M.; Lipp, H.P.; Dziembowska, M.; et al. Chronic fluoxetine treatment impairs motivation and reward learning by affecting neuronal plasticity in the central amygdala. *Br J Pharmacol* **2021**, *178*, 672–688, doi:10.1111/bph.15319.
166. Menezes, E.C.; Shah, R.; Laughlin, L.; Vinod, K.Y.; Smiley, J.F.; Cunha, C.; Balla, A.; Sershen, H.; Castellanos, F.X.; Corvelo, A.; et al. Reduced Motivation in Perinatal Fluoxetine-Treated Mice: A Hypodopaminergic Phenotype. *J Neurosci* **2021**, *41*, 2723–2732, doi:10.1523/JNEUROSCI.2608-20.2021.
167. van Mil, H.; Siegenbeek van Heukelom, J.; Bier, M. A bistable membrane potential at low extracellular potassium concentration. *Biophys Chem* **2003**, *106*, 15–21, doi:10.1016/s0301-4622(03)00135-2.
168. Williams, S.R.; Christensen, S.R.; Stuart, G.J.; Häusser, M. Membrane potential bistability is controlled by the hyperpolarization-activated current I(H) in rat cerebellar Purkinje neurons in vitro. *J Physiol* **2002**, *539*, 469–483, doi:10.1113/jphysiol.2001.013136.
169. Geukes Foppen, R.J.; van Mil, H.G.; van Heukelom, J.S. Effects of chloride transport on bistable behaviour of the membrane potential in mouse skeletal muscle. *J Physiol* **2002**, *542*, 181–191, doi:10.1113/jphysiol.2001.013298.
170. Marom, S. A Note on Bistability in a Simple Synapse-Less Point Neuron Model. *Network-Comp Neural* **1994**, *5*, 327–331, doi:10.1088/0954-898x/5/3/001.
171. Gallaher, J.; Bier, M.; van Heukelom, J.S. First order phase transition and hysteresis in a cell's maintenance of the membrane potential--An essential role for the inward potassium rectifiers. *Biosystems* **2010**, *101*, 149–155, doi:10.1016/j.biosystems.2010.05.007.
172. Law, R.; Levin, M. Bioelectric memory: modeling resting potential bistability in amphibian embryos and mammalian cells. *Theor Biol Med Model* **2015**, *12*, 22, doi:10.1186/s12976-015-0019-9.
173. Rana, M.A.; Yao, N.S.; Mukhopadhyay, S.; Zhang, F.M.; Warren, E.; Payne, C. Modeling the effect of nanoparticles & the bistability of transmembrane potential in non-excitable cells. In Proceedings of the P Amer Contr Conf, Boston, MA, 2016; pp. 400–405.
174. Cervera, J.; Alcaraz, A.; Mafe, S. Membrane potential bistability in nonexcitable cells as described by inward and outward voltage-gated ion channels. *J Phys Chem B* **2014**, *118*, 12444–12450, doi:10.1021/jp508304h.
175. Wang, L.; Walker, B.L.; Iannaccone, S.; Bhatt, D.; Kennedy, P.J.; Tse, W.T. Bistable switches control memory and plasticity in cellular differentiation. *Proc Natl Acad Sci U S A* **2009**, *106*, 6638–6643, doi:10.1073/pnas.0806137106.
176. Nishimura, K.; Kitamura, Y.; Inoue, T.; Umesono, Y.; Yoshimoto, K.; Takeuchi, K.; Taniguchi, T.; Agata, K. Identification and distribution of tryptophan hydroxylase (TPH)-positive neurons in the planarian *Dugesia japonica*. *Neurosci Res* **2007**, *59*, 101–106, doi:10.1016/j.neures.2007.05.014.
177. Saitoh, O.; Yuruzume, E.; Nakata, H. Identification of planarian serotonin receptor by ligand binding and PCR studies. *Neuroreport* **1996**, *8*, 173–178, doi:10.1097/00011756-199612200-00035.
178. Creti, P.; Capasso, A.; Grasso, M.; Parisi, E. Identification of a 5-HT1A receptor positively coupled to planarian adenylate cyclase. *Cell Biol Int Rep* **1992**, *16*, 427–432, doi:10.1016/s0309-1651(06)80062-7.
179. Cho, M.; Nayak, S.U.; Jennings, T.; Tallarida, C.S.; Rawls, S.M. Predator odor produces anxiety-like behavioral phenotype in planarians that is counteracted by fluoxetine. *Physiol Behav* **2019**, *206*, 181–184, doi:10.1016/j.physbeh.2019.04.003.
180. Welsh, J.H.; Williams, L.D. Monoamine-containing neurons in planaria. *J Comp Neurol* **1970**, *138*, 103–115, doi:10.1002/cne.901380108.
181. Umesono, Y.; Tasaki, J.; Nishimura, Y.; Hrouda, M.; Kawaguchi, E.; Yazawa, S.; Nishimura, O.; Hosoda, K.; Inoue, T.; Agata, K. The molecular logic for planarian regeneration along the anterior-posterior axis. *Nature* **2013**, *500*, 73–76, doi:10.1038/nature12359.
182. Iglesias, M.; Gomez-Skarmeta, J.L.; Salo, E.; Adell, T. Silencing of Smed-betacatenin1 generates radial-like hypercephalized planarians. *Development* **2008**, *135*, 1215–1221, doi:10.1242/dev.020289.
183. Petersen, C.P.; Reddien, P.W. Smed-betacatenin-1 is required for anteroposterior blastema polarity in planarian regeneration. *Science* **2008**, *319*, 327–330, doi:10.1126/science.1149943.
184. Fan, F.L.; Xiong, J.; Li, M.; Wang, G. On Interpretability of Artificial Neural Networks: A Survey. *IEEE Trans Radiat Plasma Med Sci* **2021**, *5*, 741–760, doi:10.1109/trpms.2021.3066428.
185. Zhang, Y.; Tiño, P.; Leonardi, A.; Tang, K. A Survey on Neural Network Interpretability. *Ieee Transactions on Emerging Topics in Computational Intelligence* **2021**, *5*, 726–742, doi:10.1109/TETCI.2021.3100641.
186. Chakraborty, S.; Tomsett, R.; Raghavendra, R.; Harborne, D.; Alzantot, M.; Cerutti, F.; Srivastava, M.; Preecce, A.; Julier, S.; Rao, R.M.; et al. Interpretability of deep learning models: A survey of results. In Proceedings of the 2017 SmartWorld Conference, San Francisco, CA, 2017, 2017; pp. 1–6.
187. Li, X.H.; Xiong, H.Y.; Li, X.J.; Wu, X.Y.; Zhang, X.; Liu, J.; Bian, J.; Dou, D.J. Interpretable deep learning: interpretation, interpretability, trustworthiness, and beyond. *Knowledge and Information Systems* **2022**, *64*, 3197–3234, doi:10.1007/s10115-022-01756-8.
188. Rotem, O.; Zaritsky, A. Visual interpretability of bioimaging deep learning models. *Nat Methods* **2024**, *21*, 1394–1397, doi:10.1038/s41592-024-02322-6.
189. Lagasse, E.; Levin, M. Future medicine: from molecular pathways to the collective intelligence of the body. *Trends Mol Med* **2023**, *29*, 687–710, doi:10.1016/j.molmed.2023.06.007.
190. Tabibzadeh, S.; Brown, O.R. Trending toward geromelectroceuticals that target membrane potential for reprogramming aging and lifespan. *Aging and Cancer* **2024**, *5*, 3–13, doi:10.1002/aac2.12070.